

NIST Special Publication 1169

**Verification and Validation
of Commonly Used
Empirical Correlations
for Fire Scenarios**

Kristopher J. Overholt

<http://dx.doi.org/10.6028/NIST.SP.1169>

NIST Special Publication 1169

Verification and Validation of Commonly Used Empirical Correlations for Fire Scenarios

Kristopher J. Overholt
*Fire Research Division
Engineering Laboratory*

<http://dx.doi.org/10.6028/NIST.SP.1169>
SVN Repository Revision : 19098

March 2014



U.S. Department of Commerce
Penny Pritzker, Secretary

National Institute of Standards and Technology
Patrick D. Gallagher, Under Secretary of Commerce for Standards and Technology and Director

Certain commercial entities, equipment, or materials may be identified in this document in order to describe an experimental procedure or concept adequately. Such identification is not intended to imply recommendation or endorsement by the National Institute of Standards and Technology, nor is it intended to imply that the entities, materials, or equipment are necessarily the best available for the purpose.

National Institute of Standards and Technology Special Publication 1169
Natl. Inst. Stand. Technol. Spec. Publ. 1169, 100 pages (March 2014)
CODEN: NSPUE2

Preface

In 2007, the U.S. Nuclear Regulatory Commission (NRC), together with the Electric Power Research Institute (EPRI) and the National Institute of Standards and Technology (NIST), conducted a research project to verify and validate five fire models that have been used for nuclear power plant (NPP) applications. The results of this effort were documented in a seven-volume report, NUREG-1824 (EPRI 1011999), *Verification and Validation of Selected Fire Models for Nuclear Power Plant Applications* [1].

In 2014, the verification and validation study was expanded, and this document was created to serve as a verification and validation guide for the empirical correlations. The full details of this expanded verification and validation study are summarized in NUREG-1824 Supplement 1 (EPRI 3002002182) [2].

The model evaluation process consists of two main components: verification and validation. Verification is a process to check the correctness of the solution of the governing equations. Verification does not imply that the governing equations are appropriate; only that the equations are being solved correctly.

Validation is a process to determine the appropriateness of the governing equations as a mathematical model of the physical phenomena of interest. Typically, validation involves comparing model results with experimental measurement. Differences that cannot be attributed to uncertainty in the measured quantities in the experiment are attributed to the assumptions and simplifications of the physical model.

Contents

Preface	iii
Contents	v
List of Figures	vii
List of Tables	ix
List of Acronyms	xi
1 Introduction	1
1.1 Scope of this Document	1
1.2 Organization of this Document	2
1.3 List of Experimental Data Sets	2
2 Hot Gas Layer Temperature	3
2.1 Natural Ventilation (MQH)	3
2.2 Forced Ventilation (FPA)	7
2.3 Forced Ventilation (DB)	10
2.4 No Ventilation (Beyler)	13
3 Hot Gas Layer Depth	17
3.1 ASET Method	17
3.2 Yamana and Tanaka Method	20
4 Plume Temperature	23
4.1 Heskestad Method	23
4.2 McCaffrey Method	26
5 Target Temperature	29
5.1 Cable Failure Time	29
5.2 Unprotected Steel Temperature	33
5.3 Protected Steel Temperature	35
6 Target Heat Flux	39
6.1 Point Source Radiation Heat Flux	39
6.2 Solid Flame Radiation Heat Flux	42
7 Ceiling Jet Temperature	47

8	Sprinkler Activation Time	51
9	Smoke Detector Activation Time	55
10	Summary	59
	Bibliography	61
A	Validation Input Parameters	65
A.1	ATF Corridors	65
A.2	CAROLFIRE	66
A.3	Fleury Heat Flux	69
A.4	FM/SNL	70
A.5	LLNL Enclosure	73
A.6	NBS Multi-Room	76
A.7	NIST/NRC	77
A.8	NIST Smoke Alarms	80
A.9	SP AST	82
A.10	SP AST Column	85
A.11	Steckler	87
A.12	UL/NFPRF	89
A.13	USN Hawaii	91
A.14	USN Iceland	92
A.15	Vettori Flat Ceiling	93
A.16	VTT Large Hall	95
A.17	WTC	96

List of Figures

2.1 Summary of HGL temperature predictions for natural ventilation tests (MQH)	5
2.2 Summary of HGL temperature predictions for forced ventilation tests (FPA)	9
2.3 Summary of HGL temperature predictions for forced ventilation tests (DB)	12
2.4 Summary of HGL temperature predictions for no ventilation tests (Beyler)	15
3.1 Summary of HGL depth predictions (ASET)	19
3.2 Summary of HGL depth predictions (Yamana and Tanaka)	22
4.1 Summary of plume temperature predictions (Heskestad)	25
4.2 Summary of plume temperature predictions (McCaffrey)	28
5.1 Summary of cable failure time predictions	32
5.2 Summary of target temperature predictions	38
6.1 Summary of point source radiation heat flux predictions	41
6.2 Summary of solid flame radiation heat flux predictions	45
7.1 Summary of ceiling jet temperature predictions	50
8.1 Summary of sprinkler activation time predictions	53
9.1 Summary of smoke detector activation time predictions (Temperature Rise)	57

List of Tables

1.1	Experimental data sets used in this validation study	2
2.1	Verification case, HGL temperature, natural ventilation	4
2.2	Verification case, HGL temperature, forced ventilation	8
2.3	Verification case, HGL temperature, forced ventilation	11
2.4	Verification case, HGL temperature, no ventilation	14
3.1	Verification case, HGL depth	18
3.2	Verification case, HGL depth	21
4.1	Verification case, plume temperature	24
4.2	Constants used in McCaffrey plume temperature correlation	26
4.3	Verification case, plume temperature	27
5.1	Verification case, cable failure time	31
5.2	Verification case, unprotected steel temperature	34
5.3	Verification case, protected steel temperature	36
5.4	Verification case, protected steel temperature (continued)	37
6.1	Verification case, point source radiation heat flux	40
6.2	Verification case, solid flame radiation heat flux	44
7.1	Verification case, ceiling jet temperature	48
8.1	Verification case, sprinkler activation time	52
9.1	Verification case, smoke detector activation time	56
10.1	Summary statistics	59
A.1	Validation input parameters for ATF Corridors cases, ceiling jet temperature	65
A.2	Validation input parameters for CAROLFIRE cases, cable failure time	67
A.3	Validation input parameters for CAROLFIRE cases, cable failure time (continued)	68
A.4	Validation input parameters for Fleury Heat Flux cases, radiation heat flux	69
A.5	Validation input parameters for FM/SNL cases, HGL temperature	70
A.6	Validation input parameters for FM/SNL cases, plume temperature	71
A.7	Validation input parameters for FM/SNL cases, ceiling jet temperature	72
A.8	Validation input parameters for LLNL Enclosure cases, HGL temperature	74
A.9	Validation input parameters for NBS Multi-Room cases, HGL temperature	76
A.10	Validation input parameters for NIST/NRC cases, HGL temperature and depth	77
A.11	Validation input parameters for NIST/NRC cases, radiation heat flux	78

A.12	Validation input parameters for NIST/NRC cases, ceiling jet temperature	79
A.13	Validation input parameters for NIST Smoke Alarms cases, ceiling jet temperature	80
A.14	Validation input parameters for NIST Smoke Alarms cases, smoke detector activation time	81
A.15	Validation input parameters for SP AST cases, HGL temperature	82
A.16	Validation input parameters for SP AST cases, unprotected steel temperature	83
A.17	Validation input parameters for SP AST cases, ceiling jet temperature	84
A.18	Validation input parameters for SP AST Column cases, plume temperature	85
A.19	Validation input parameters for SP AST Column cases, unprotected steel temperature	86
A.20	Validation input parameters for Steckler cases, HGL temperature	87
A.21	Validation input parameters for UL/NFPRF cases, ceiling jet temperature	89
A.22	Validation input parameters for UL/NFPRF cases, sprinkler activation time	90
A.23	Validation input parameters for USN Hawaii cases, plume temperature	91
A.24	Validation input parameters for USN Hawaii cases, plume temperature	92
A.25	Validation input parameters for Vettori Flat cases, ceiling jet temperature	93
A.26	Validation input parameters for Vettori Flat cases, sprinkler activation time	94
A.27	Validation input parameters for VTT Large Hall cases, plume temperature	95
A.28	Validation input parameters for WTC cases, HGL temperature	96
A.29	Validation input parameters for WTC cases, unprotected steel temperature	97
A.30	Validation input parameters for WTC cases, protected steel temperature	98
A.31	Validation input parameters for WTC cases, radiation heat flux	99
A.32	Validation input parameters for WTC cases, ceiling jet temperature	100

List of Acronyms

AST	Adiabatic Surface Temperature
ATF	Bureau of Alcohol, Tobacco, Firearms, and Explosives
CAROLFIRE	Cable Response to Live Fire Test Program
CFAST	Consolidated Model of Fire Growth and Smoke Transport
FDS	Fire Dynamics Simulator
FM	Factory Mutual Global
HGL	Hot Gas Layer
HRR	Heat Release Rate
LLNL	Lawrence Livermore National Laboratory
NBS	National Bureau of Standards (former name of NIST)
NFPRF	National Fire Protection Research Foundation
NIST	National Institute of Standards and Technology
NRC	Nuclear Regulatory Commission
RTI	Response Time Index
SNL	Sandia National Laboratory
SP	Statens Provningsanstalt (Technical Research Institute of Sweden)
THIEF	Thermally-Induced Electrical Failure
UL	Underwriters Laboratories
USN	United States Navy
VTT	Valtion Teknillinen Tutkimuskeskus (Technical Research Centre of Finland)
WTC	World Trade Center

Chapter 1

Introduction

1.1 Scope of this Document

Various empirical correlations exist for calculating quantities of interest related to fire dynamics in a compartment (e.g., hot gas layer temperature, heat flux, plume temperature). The focus of this document is to compare predictions made using empirical correlations to various experimentally measured quantities for a fire in a compartment and to express the accuracy and uncertainty of the predictions in a consistent manner. The empirical correlations selected for use in this document are based on the correlations that are used in nuclear power plant (NPP) applications, and more details are provided in the verification and validation report, NUREG-1824 Supplement 1 (EPRI 3002002182) [2].

A Fortran program was developed along with this document that implements the calculations for the empirical correlations and automates the verification and validation process. This automated verification and validation process is a method for maintaining the empirical correlations in the long term in a centralized location and enables model verification and validation to be performed on the empirical correlations in a systematic manner. As new empirical correlations are developed or relevant compartment fire experiments are conducted, they can be added to this verification and validation suite and documented.

This document is complementary to the verification and validation guides for the Consolidated Model of Fire Growth and Smoke Transport (CFAST) [3] and Fire Dynamics Simulator (FDS) [4, 5]. The experiments referred to in this study are described in more detail in the FDS Validation Guide [5] (Volume 3 of the FDS Technical Reference Guide) and their respective test reports. The source code for the empirical correlations calculation program, the verification and validation scripts used to generate this document, and the experimental data shown in this document are freely available for download from the primary website for FDS.¹

¹<http://fire.nist.gov/fds>

1.2 Organization of this Document

For each quantity and empirical correlation, Sections 2 through 9 provide a short description of the governing equations, a verification example, and a validation scatter plot that shows model predictions compared to measured values. For each empirical correlation, the corresponding validation scatter plot lists the experimental relative standard deviation, model relative standard deviation, and bias factor.

Section 10 includes a table of summary statistics for each quantity and empirical correlation. These statistical metrics can be used to summarize the uncertainty of model predictions and the tendency of a model to underpredict or overpredict a given quantity. More detailed discussion on the application and usage of these statistical metrics is provided in the “Quantifying Model Uncertainty” chapter of the FDS Validation Guide [5].

For each of the experimental data sets, Appendix A lists the input parameters for the empirical correlations that were used in each of the the validation cases.

1.3 List of Experimental Data Sets

The experimental data sets included in this validation study are shown in Table 1.1. The experiments are described in more detail in the FDS Validation Guide [5] (Volume 3 of the FDS Technical Reference Guide) and their respective test reports.

Table 1.1: Experimental data sets used in this validation study.

Test Series	Description	Reference
ATF Corridors	Gas burner tests in a two-story structure with long hallways	[6]
CAROLFIRE	Electrical cables within a heated test apparatus	[7]
Fleury Heat Flux	Propane burner tests with measured heat flux	[8]
FM/SNL	Gas and liquid pool fire tests with forced ventilation	[9, 10]
LLNL Enclosure	Methane burner tests with various ventilation conditions	[11]
NBS Multi-Room	Gas burner tests in a three-room suite and corridor	[12]
NIST/NRC	Liquid spray burner tests with various ventilation conditions	[13]
NIST Smoke Alarms	Single-story manufactured home with furniture fire tests	[14]
SP AST	Gas burner tests in a compartment with a horizontal beam	[15]
SP AST Column	Pool fire tests with a vertical column in the center	[16]
Steckler	Compartment fire tests conducted at NBS (NIST)	[17]
UL/NFPRF	Spray burner tests in a large-scale facility with sprinklers	[18, 19]
USN Hawaii	Jet fuel fire tests in an aircraft hangar in a warm climate	[20]
USN Iceland	Jet fuel fire tests in an aircraft hangar in a cold climate	[20]
Vettori Flat Ceiling	Compartment tests conducted at NIST with residential sprinklers	[21]
VTT Large Hall	Heptane pool fire tests in a large-scale facility	[22]
WTC	Compartment spray burner tests conducted at NIST	[23]

Chapter 2

Hot Gas Layer Temperature

The empirical correlations can predict an average hot gas layer (HGL) temperature. Because there are different empirical correlations for compartments that are naturally ventilated, mechanically ventilated, or unventilated, the results for HGL temperature are divided into three categories.

2.1 Natural Ventilation (MQH)

Description

For a compartment with natural ventilation, the correlation of McCaffrey, Quintiere, and Harkleroad (MQH) [24] predicts that the hot gas layer (HGL) temperature rise, ΔT_g ($^{\circ}\text{C}$), is given by

$$\Delta T_g = 6.85 \left(\frac{\dot{Q}^2}{A_o \sqrt{H_o} h_k A_T} \right)^{1/3} \quad (2.1)$$

where \dot{Q} is the total heat release rate (HRR) of the fire (kW), A_o is the area of the ventilation opening (m^2), H_o is the height of the ventilation opening (m), and A_T is the total area of the compartment enclosing surfaces (m^2), excluding areas of vent openings, which is given by

$$A_T = 2LW + 2LH + 2WH - H_o W_o \quad (2.2)$$

where L , W , H are the length, width, and height of the compartment (m), respectively, and W_o is the width of the ventilation opening (m). The heat transfer coefficient, h_k ($\text{kW}/(\text{m}^2 \cdot \text{K})$), is given by

$$h_k = \begin{cases} \sqrt{k\rho c/t} & t \leq t_p \\ k/\delta & t > t_p \end{cases} \quad (2.3)$$

where k is the thermal conductivity of the interior lining ($\text{kW}/(\text{m} \cdot \text{K})$), ρ is its density (kg/m^3), c is its specific heat ($\text{kJ}/(\text{kg} \cdot \text{K})$), and δ is its thickness (m). The thermal penetration time, t_p (s), is given by

$$t_p = \left(\frac{\rho c}{k} \right) \left(\frac{\delta}{2} \right)^2 \quad (2.4)$$

Verification

This example case is based on Test 51 from the Lawrence-Livermore National Laboratory (LLNL) [11] series. This test involved a compartment with an open door, a methane burner, and natural ventilation.

Table 2.1: Verification case, HGL temperature, natural ventilation.

User-Specified Input	
Parameter	Value
\dot{Q} (kW)	200
L (m)	6.0
W (m)	4.0
H (m)	3.0
H_o (m)	2.06
W_o (m)	0.76
k (kW/(m · K))	0.000463
ρ (kg/m ³)	1607
c (kJ/(kg · K))	1.0
δ (m)	0.10
T_∞ (°C)	33

Calculated Output	
Time (s)	HGL Temperature (°C)
0	33.00
60	111.45
120	121.05
180	127.21
600	148.14
1200	162.24
1800	171.28
2400	178.07
3000	183.57

This verification example serves as both a worked example case and a check on the mathematical implementation of this empirical correlation for software quality assurance (SQA) purposes, hence the extended number of significant digits. The verification examples are similar for all of the remaining empirical correlations in this document.

Validation

A summary of the comparisons between peak predicted and measured compartment temperatures is shown in Fig. 2.1.

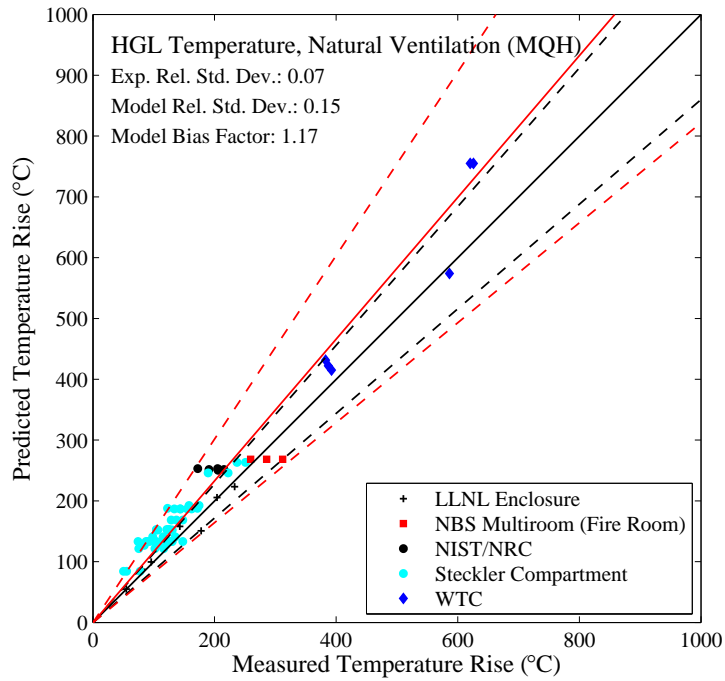


Figure 2.1: Summary of HGL temperature predictions for natural ventilation tests using the MQH method.

Explanation of Statistical Metrics

In Fig. 2.1, the measured values are represented by the horizontal axis and the predicted values by the vertical axis. If a particular prediction and measurement are the same, then the resulting point falls on the solid diagonal line. To better make use of these results, two statistical parameters are calculated for each empirical correlation and each predicted quantity. The first parameter, δ , is the bias factor, which indicates the extent to which the empirical correlation, on average, under or over-predicts the measurements of a given quantity. It is assumed that the experiments are unbiased; that is, the bias factor for the experimental measurements is 1. For example, a bias factor of 1.02 indicates that the model over-estimates the measured quantity by 2 %, on average. The bias factor is shown graphically by the solid red line.

The second parameter, $\tilde{\sigma}_M$, is the relative standard deviation of the model, which indicates the variability of the model. In Fig. 2.1, there are two sets of off-diagonal lines. The first set, shown as dashed black lines, indicate the uncertainty of the experimental measurements in terms of a relative standard deviation, $\tilde{\sigma}_E$. The experimental relative standard deviation was determined by considering the systematic and random uncertainty values for each measurement quantity, which is described in more detail in the “Experimental Uncertainty” section of the FDS Validation Guide [5]. The slopes of the dashed black lines are $1 \pm 2\tilde{\sigma}_E$, which represents the 95 % confidence intervals. The set of red dashed lines indicate the model relative standard deviation, $\tilde{\sigma}_M$. The model relative standard deviation is reported as one standard deviation of the predicted quantity. The slopes of these lines are $\delta \pm 2\tilde{\sigma}_M$. If the model was as accurate as the measurements against which it is compared, then the two sets of off-diagonal lines would merge. The extent to which the data scatters outside of the experimental bounds is an indication of the degree of uncertainty of the empirical correlations.

These symbols and nomenclature are similar for all of the remaining scatter plots in this document. More detailed discussion of the experimental and model relative standard deviations is provided in the FDS Validation Guide [5] and in McGrattan and Toman [25].

2.2 Forced Ventilation (FPA)

Description

For a compartment with forced ventilation, the correlation of Foote, Pagni, and Alvares (FPA) [24] predicts that the HGL temperature rise, ΔT_g ($^{\circ}\text{C}$), is given by

$$\Delta T_g = \left[0.63 \left(\frac{\dot{Q}}{\dot{m}_g c_p T_{\infty}} \right)^{0.72} \left(\frac{h_k A_T}{\dot{m}_g c_p} \right)^{-0.36} \right] T_{\infty} \quad (2.5)$$

where \dot{Q} is the HRR of the fire (kW), \dot{m}_g is the compartment ventilation mass flow rate (kg/s), c_p is the specific heat of air (kJ/(kg·K)), T_{∞} is the ambient air temperature ($^{\circ}\text{C}$), h_k is the heat transfer coefficient (kW/($\text{m}^2 \cdot \text{K}$)), and A_T is the total area of the compartment enclosing surfaces (m^2), excluding areas of vent openings. The heat transfer coefficient, h_k (kW/($\text{m}^2 \cdot \text{K}$)), is given by

$$h_k = \begin{cases} \sqrt{k\rho c/t} & t \leq t_p \\ k/\delta & t > t_p \end{cases} \quad (2.6)$$

where k is the thermal conductivity of the interior lining (kW/($\text{m} \cdot \text{K}$)), ρ is its density (kg/m^3), c is its specific heat (kJ/($\text{kg} \cdot \text{K}$)), and δ is its thickness (m). The thermal penetration time, t_p (s), is given by

$$t_p = \left(\frac{\rho c}{k} \right) \left(\frac{\delta}{2} \right)^2 \quad (2.7)$$

Verification

This example case is based on Test 1 from the Factory Mutual and Sandia National Laboratories (FM/SNL) [9, 10] series. This test involved a compartment with an open door, a propylene burner, and forced ventilation.

Table 2.2: Verification case, HGL temperature, forced ventilation.

User-Specified Input	
Parameter	Value
\dot{Q} (kW)	516
\dot{m} (kg/s)	4.5
c_p (kJ/(kg · K))	1.0
L (m)	18.3
W (m)	12.2
H (m)	6.1
k (kW/(m · K))	0.00023
ρ (kg/m ³)	1000
c (kJ/(kg · K))	1.16
δ (m)	0.025
T_∞ (°C)	15

Calculated Output	
Time (s)	HGL Temperature (°C)
0	15.00
60	53.07
120	58.13
180	61.39
240	63.86
300	65.86
360	67.56
420	69.04
480	70.35
540	71.54
600	72.62

Validation

A summary of the comparisons between peak predicted and measured compartment temperatures is shown in Fig. 2.2.

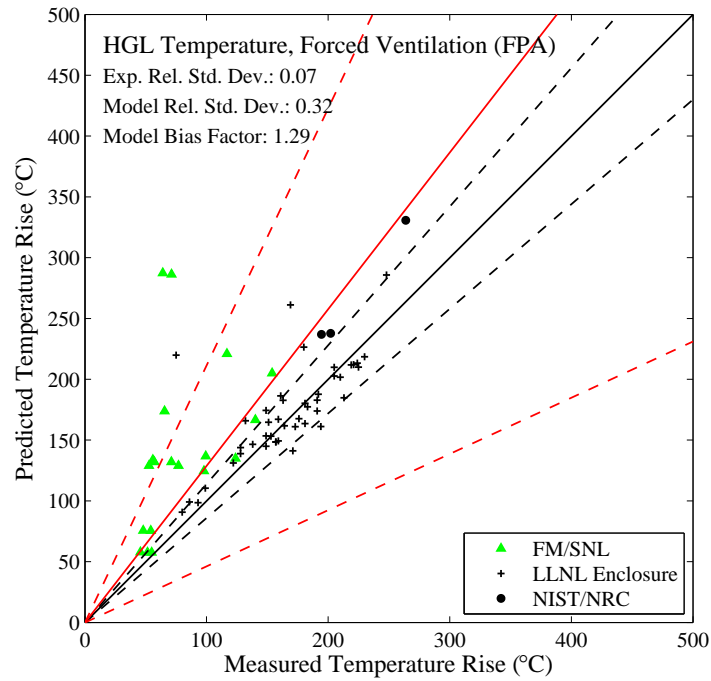


Figure 2.2: Summary of HGL temperature predictions for forced ventilation tests using the FPA method.

Note that the LLNL Enclosure experiments were used to develop the FPA correlation.

2.3 Forced Ventilation (DB)

Description

For a compartment with forced ventilation, the correlation of Deal and Beyler (DB) [24] predicts that the HGL temperature rise, ΔT_g ($^{\circ}\text{C}$), is given by

$$\Delta T_g = \left(\frac{\dot{Q}}{\dot{m}_g c_p + h_k A_T} \right) \quad (2.8)$$

where \dot{Q} is the HRR of the fire (kW), \dot{m}_g is the compartment ventilation mass flow rate (kg/s), c_p is the specific heat of air (kJ/(kg · K)), T_{∞} is the ambient air temperature ($^{\circ}\text{C}$), h_k is the heat transfer coefficient (kW/(m² · K)), and A_T is the total area of compartment enclosing surfaces (m²), excluding areas of vent openings. The heat transfer coefficient, h_k (kW/(m² · K)), is given by

$$h_k = 0.4 \max \left(\sqrt{\frac{k\rho c}{t}}, \frac{k}{\delta} \right) \quad (2.9)$$

where k is the thermal conductivity of the interior lining (kW/(m · K)), ρ is the density of the interior lining (kg/m³), c is the specific heat of the interior lining (kJ/(kg · K)), t is the exposure time (s), and δ is the thickness of the interior lining (m). This model is only valid for times up to 2000 seconds.

Verification

This example case is based on Test 1 from the Factory Mutual and Sandia National Laboratories (FM/SNL) [9, 10] series. This test involved a compartment with an open door, a propylene burner, and forced ventilation.

Table 2.3: Verification case, HGL temperature, forced ventilation.

User-Specified Input	
Parameter	Value
\dot{Q} (kW)	516
\dot{m} (kg/s)	4.5
c_p (kJ/(kg · K))	1.0
L (m)	18.3
W (m)	12.2
H (m)	6.1
k (kW/(m · K))	0.00023
ρ (kg/m ³)	1000
c (kJ/(kg · K))	1.16
δ (m)	0.025
T_∞ (°C)	15

Calculated Output	
Time (s)	HGL Temperature (°C)
0	15.00
60	34.60
120	40.88
180	45.16
240	48.47
300	51.17
360	53.47
420	55.46
480	57.23
540	58.81
600	60.24

Validation

A summary of the comparisons between peak predicted and measured compartment temperatures is shown in Fig. 2.3.

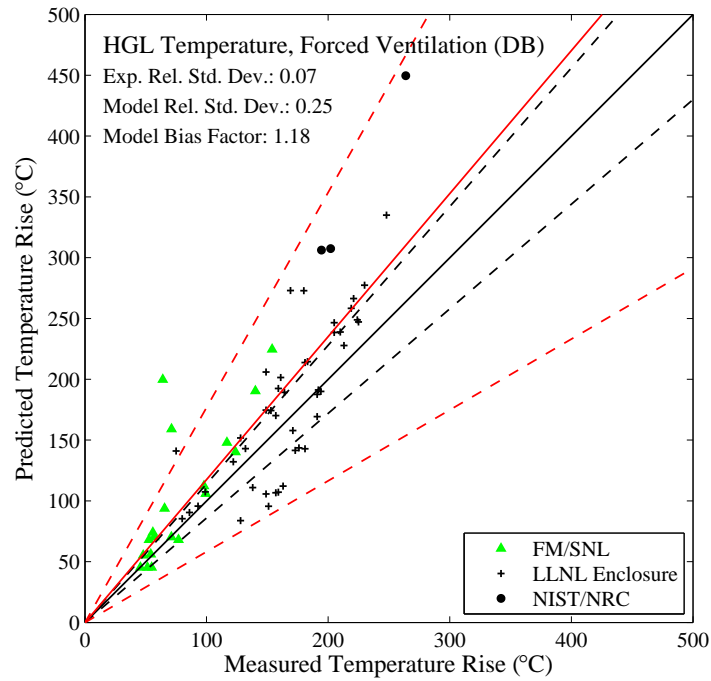


Figure 2.3: Summary of HGL temperature predictions for forced ventilation tests using the DB method.

2.4 No Ventilation (Beyler)

Description

For a compartment with no ventilation (closed doors) and constant HRR, the correlation of Beyler [24] predicts that the HGL temperature rise, ΔT_g ($^{\circ}\text{C}$), is given by

$$\Delta T_g = \frac{2K_2}{K_1^2} (K_1 \sqrt{t} - 1 + e^{-K_1 \sqrt{t}}) \quad (2.10)$$

where t is the exposure time (s). K_1 is given by

$$K_1 = \frac{2(0.4\sqrt{k\rho c})A_T}{mc_p} \quad (2.11)$$

where k is the thermal conductivity of the interior lining ($\text{kW}/(\text{m} \cdot \text{K})$), ρ is the density of the interior lining (kg/m^3), c is the specific heat of the interior lining ($\text{kJ}/(\text{kg} \cdot \text{K})$), A_T the total area of compartment enclosing surfaces (m^2), m is the mass of gas in the compartment (kg), and c_p is the specific heat of air ($\text{kJ}/(\text{kg} \cdot \text{K})$). K_2 is given by

$$K_2 = \frac{\dot{Q}}{mc_p} \quad (2.12)$$

where \dot{Q} is the HRR of the fire (kW).

Verification

This example case is based on Test 1 from the Lawrence-Livermore National Laboratory (LLNL) [11] series. This test involved a compartment with an open door, a methane burner, and no ventilation.

Table 2.4: Verification case, HGL temperature, no ventilation.

User-Specified Input	
Parameter	Value
\dot{Q} (kW)	200
L (m)	6.0
W (m)	4.0
H (m)	4.5
c_p (kJ/(kg · K))	1.0
k (kW/(m · K))	0.000463
ρ (kg/m ³)	1607
c (kJ/(kg · K))	1.0
T_∞ (°C)	23

Calculated Output	
Time (s)	HGL Temperature (°C)
0	23.00
100	59.33
200	76.72
300	90.07
400	101.33
500	111.24

Validation

A summary of the comparisons between peak predicted and measured compartment temperatures is shown in Fig. 2.4.

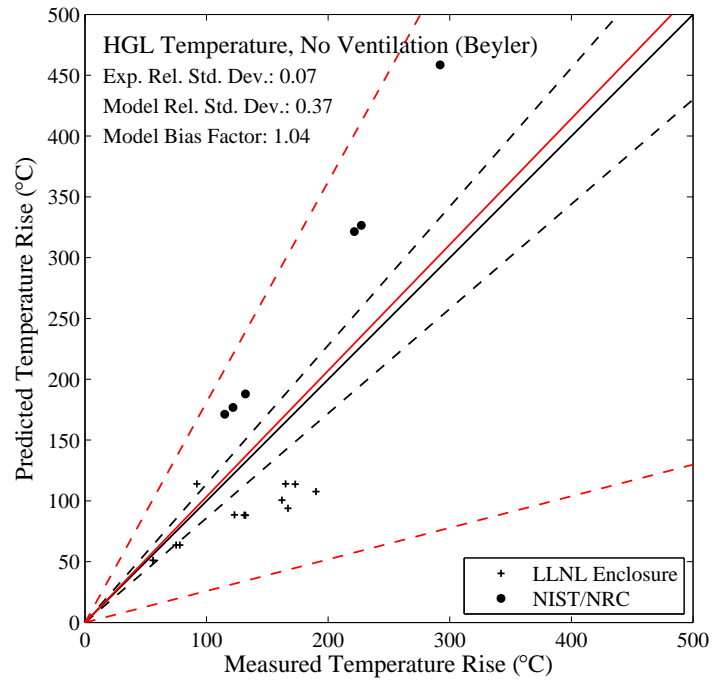


Figure 2.4: Summary of HGL temperature predictions for no ventilation tests using the Beyler method.

Chapter 3

Hot Gas Layer Depth

The HGL depth is defined as the distance between the ceiling and the HGL height.

3.1 ASET Method

Description

For a compartment with no ventilation (closed doors) and constant HRR, the available safe egress time (ASET) [26] correlation predicts that the HGL height, z (m), is given by [27]

$$A_s \frac{dz}{dt} = \frac{dV_{ul}}{dt} = \dot{V}_{ul} \quad (3.1)$$

where A_s is the area of the boundary surfaces (m^2), and V_{ul} is the volume of the HGL (m^3). The change in volume of the upper layer, \dot{V}_{ul} (m^3/s), is given by

$$\dot{V}_{ul} = \dot{V}_{exp} + \dot{V}_{ent} \quad (3.2)$$

The volumetric expansion rate, \dot{V}_{exp} (m^3/s), is given by [28]

$$\dot{V}_{exp} = \frac{\dot{Q}_{net}}{\rho_g c_p T_g} \approx \frac{(1 - \chi_l) \dot{Q}_f}{353} \quad ; \quad \dot{Q}_{net} = \dot{Q}_f - \dot{Q}_l = \dot{Q}_f(1 - \chi_l) \quad (3.3)$$

where \dot{Q}_{net} , \dot{Q}_f , and \dot{Q}_l are the net HRR, total HRR, and HRR loss to the boundaries (kW), respectively, ρ_g , c_p and T_g are the density (kg/m^3), specific heat ($kJ/(kg \cdot K)$), and temperature (K) of air in the HGL, respectively, and χ_l is the heat loss fraction to the enclosure boundaries. The volumetric entrainment rate, \dot{V}_{ent} (m^3/s), is given by [29]

$$\dot{V}_{ent} = k_v \dot{Q}^{1/3} z^{5/3} = \frac{0.21}{K_f} \left(\frac{g}{\rho_\infty T_\infty} \right)^{1/3} (K_f \dot{Q})^{1/3} (z - z_f)^{5/3} \quad (3.4)$$

where k_v is the volumetric entrainment coefficient, g is the acceleration due to gravity (m/s^2), ρ_∞ and T_∞ are the density (kg/m^3) and temperature (K) of ambient air, respectively, K_f is the location factor, and z_f is the fuel height (m). The location factor has a value of 1, 2, or 4, which corresponds to a fire away from walls or corners, a fire adjacent to a wall, or a fire located in a corner, respectively.

The HGL height, z , in Eq. 3.1 can be calculated iteratively using

$$z|_{t+1} = z|_t - \frac{\dot{V}_{ul}}{LW} \Delta t \quad (3.5)$$

where L and W are the length and width of the compartment (m), respectively, and Δt is the time step size (s).

Verification

This example case is based on Test 1 from the NIST and Nuclear Regulatory Commission (NIST/NRC) [13] series. This test involved a compartment with a closed door, a heptane spray burner, and no ventilation.

Table 3.1: Verification case, HGL depth.

User-Specified Input	
Parameter	Value
\dot{Q} (kW)	410
L (m)	21.66
W (m)	7.04
H (m)	3.82
k (kW/(m · K))	0.00012
ρ (kg/m ³)	737
c (kJ/(kg · K))	1.42
T_{∞} (°C)	22
Location Factor	1
χ_l	0
z_f	0

Calculated Output	
Time (s)	HGL Depth (m)
0	0.00
10	0.35
20	0.65
30	0.93
40	1.17
50	1.40
60	1.60
100	2.26
200	3.34
300	3.82
1000	3.82
1350	3.82

Validation

A summary of the comparisons between peak predicted and measured HGL depths is shown in Fig. 3.1.

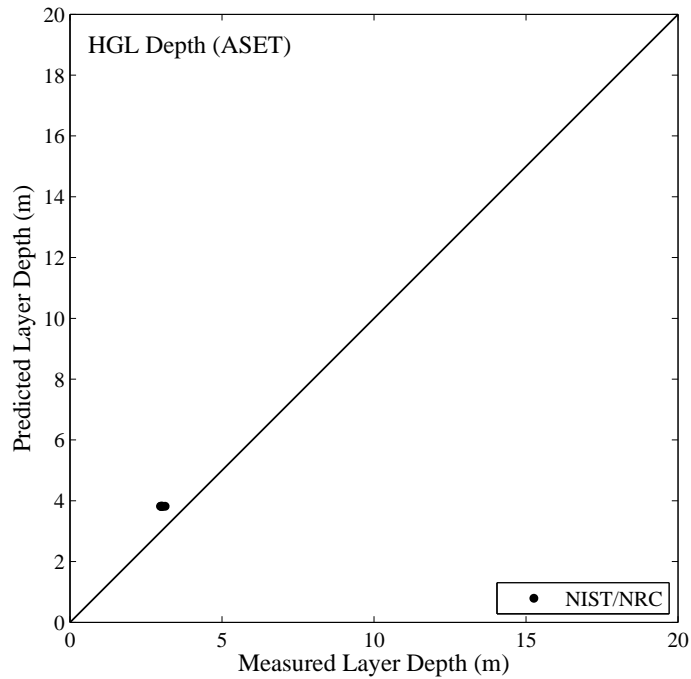


Figure 3.1: Summary of HGL depth predictions using ASET.

This correlation is only valid for closed room tests, and the NIST/NRC tests are the only closed room data set with reduced HGL depth data. Note that the bias and standard deviation are not calculated for these cases because of the limited amount of data.

3.2 Yamana and Tanaka Method

Description

For a compartment with no ventilation (closed doors) and constant HRR, the correlation of Yamana and Tanaka [30] predicts that the HGL height, z (m), is given by

$$z = \left(\frac{2k\dot{Q}^{1/3}t}{3A_c} + \frac{1}{h_c^{2/3}} \right)^{-3/2} \quad (3.6)$$

where \dot{Q} is the HRR (kW), t is the time after ignition (s), A_c is the compartment floor area (m²), and h_c is the compartment height (m). The constant k is given by

$$k = \frac{0.076}{(353/T_g)} \quad (3.7)$$

where T_g is the HGL temperature (K).

Verification

This example case is based on Test 1 from the NIST and Nuclear Regulatory Commission (NIST/NRC) [13] series. This test involved a compartment with a closed door, a heptane spray burner, and no ventilation.

Note: In this verification case, the Beyler method (see Section 2.4) is used to calculate the HGL temperature, T_g .

Table 3.2: Verification case, HGL depth.

User-Specified Input	
Parameter	Value
\dot{Q} (kW)	410
L (m)	21.66
W (m)	7.04
H (m)	3.82
k (kW/(m · K))	0.00012
ρ (kg/m ³)	737
c (kJ/(kg · K))	1.42
T_∞ (°C)	22

Calculated Output	
Time (s)	HGL Depth (m)
0	0.00
10	0.28
20	0.53
30	0.75
40	0.96
50	1.15
60	1.31
100	1.86
200	2.64
300	3.04
1000	3.67
1350	3.73

Validation

A summary of the comparisons between peak predicted and measured HGL depths is shown in Fig. 3.2.

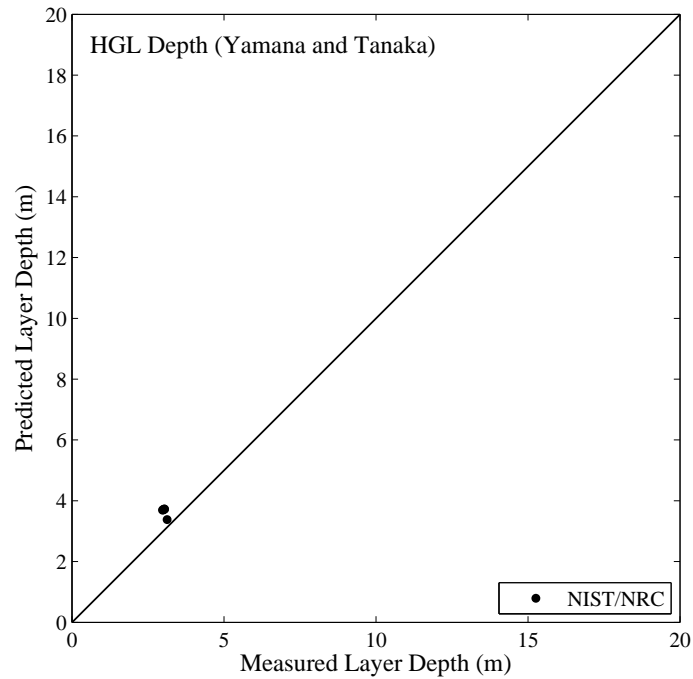


Figure 3.2: Summary of HGL depth predictions using Yamana and Tanaka method.

This correlation is only valid for closed room tests, and the NIST/NRC tests are the only closed room data set with reduced HGL depth data. Note that the bias and standard deviation are not calculated for these cases because of the limited amount of data.

Chapter 4

Plume Temperature

The fire plume transports hot gases into the HGL. Its temperature is greater than the ceiling jet and HGL temperature. It is particularly important scenarios that involve targets directly above a potential fire.

4.1 Heskestad Method

Description

For a fire plume, the correlation by Heskestad [31] predicts that the increase in centerline temperature, ΔT_0 ($^{\circ}\text{C}$), is given by

$$\Delta T_0 = \frac{9.1 \left(\frac{T_{\infty}}{g c_p^2 \rho_{\infty}^2} \right)^{1/3} \dot{Q}_c^{2/3}}{(z - z_0)^{5/3}} \quad (4.1)$$

where T_{∞} is the ambient air temperature ($^{\circ}\text{C}$), g is the acceleration of gravity (m/s^2), c_p is the specific heat of air ($\text{kJ}/(\text{kg} \cdot \text{K})$), ρ_{∞} is the ambient air density (kg/m^3), and z is the elevation above the fire source (m). The convective HRR, \dot{Q}_c (kW), is given by

$$\dot{Q}_c = \dot{Q}(1 - \chi_r) \quad (4.2)$$

where \dot{Q} is the total HRR (kW), and χ_r is the radiative fraction. Note that the total HRR \dot{Q} is the actual HRR, not the idealized HRR. The hypothetical virtual origin of the fire, z_0 (m), is given by

$$z_0 = -1.02D + 0.083\dot{Q}^{2/5} \quad (4.3)$$

where D is the diameter of the fire source (m) and is given by

$$D = \sqrt{\frac{4A}{\pi}} \quad (4.4)$$

where A is the area of the fire source (m^2). Note that this plume temperature correlation is only valid above the mean flame height.

Verification

This example case is based on Test 1 from the VTT [22] series. This test involved a large test hall with closed doors, a heptane pool fire, and no ventilation.

Table 4.1: Verification case, plume temperature.

User-Specified Input	
Parameter	Value
\dot{Q} (m)	1245
c_p (kJ/(kg · K))	1.0
z (m)	6
A (m ²)	1.075
χ_r	0.40
T_∞ (°C)	22

Calculated Output
Plume Temperature (°C)
133.78

Validation

A summary of the comparisons between peak predicted and measured plume temperatures is shown in Fig. 4.1.

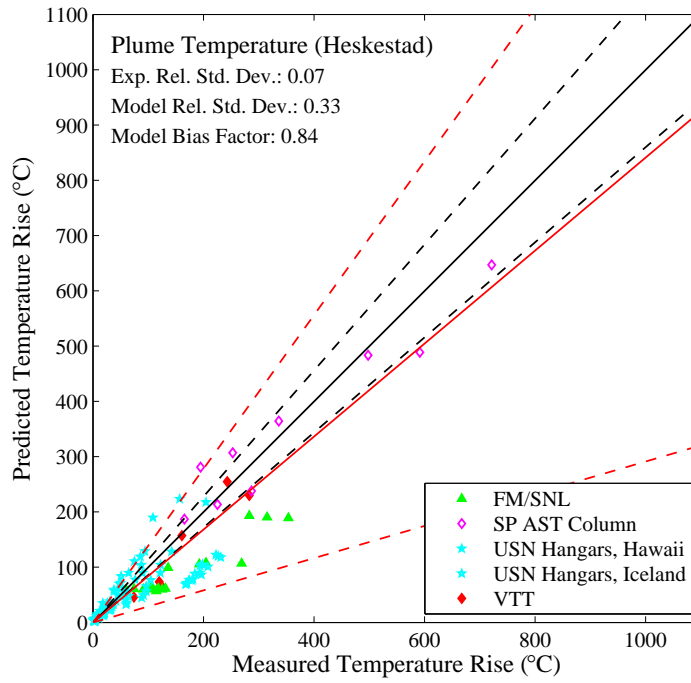


Figure 4.1: Summary of plume temperature predictions using the Heskestad method.

4.2 McCaffrey Method

Description

For a fire plume, the correlation by McCaffrey [32] predicts that the increase in centerline temperature, ΔT_0 ($^{\circ}\text{C}$), is given by

$$\Delta T_0 = \left[\left(\frac{\kappa}{0.9\sqrt{2g}} \right)^2 \left(\frac{z}{\dot{Q}^{2/5}} \right)^{2\eta-1} \right] T_{\infty} \quad (4.5)$$

where g is the acceleration of gravity (m/s^2), z is the elevation above the fire source (m), \dot{Q} is the HRR (kW), and T_{∞} is the ambient air temperature ($^{\circ}\text{C}$). The constants η and κ are a function of the height z within the plume and are listed in Table 4.2.

Table 4.2: Constants used in McCaffrey plume temperature correlation.

Region	$z/\dot{Q}^{2/5}$	η	κ
Continuous	< 0.08	1/2	6.8
Intermittent	$< 0.08 - 0.2$	0	1.9
Plume	> 0.2	-1/3	1.1

Verification

This example case is based on Test 1 from the VTT [22] series. This test involved a large test hall with closed doors, a heptane pool fire, and no ventilation.

Table 4.3: Verification case, plume temperature.

User-Specified Input	
Parameter	Value
\dot{Q} (m)	1245
z (m)	6
T_{∞} (°C)	22

Calculated Output
Plume Temperature (°C)
153.21

Validation

A summary of the comparisons between peak predicted and measured plume temperatures is shown in Fig. 4.2.

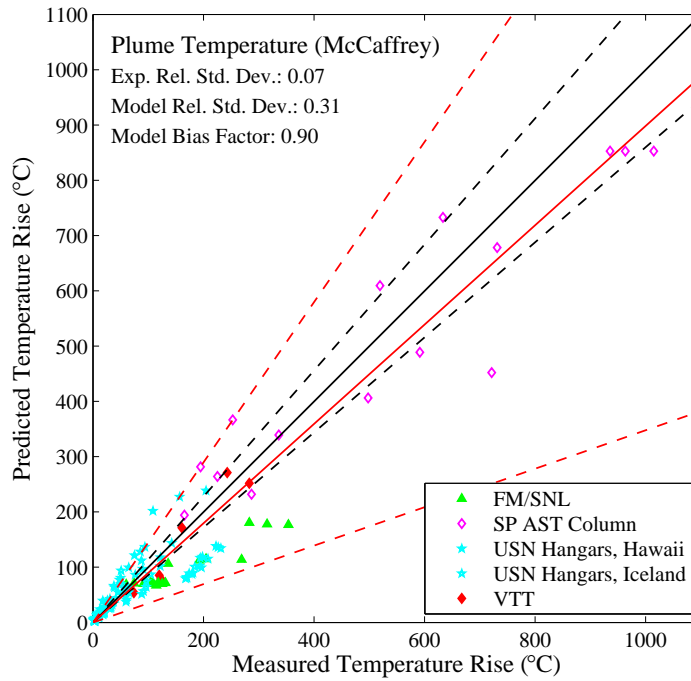


Figure 4.2: Summary of plume temperature predictions using the McCaffrey method.

Chapter 5

Target Temperature

The calculation of target temperature is a common objective of fire modeling analyses. The targets in this validation study include electrical cables as well as unprotected and protected steel members.

5.1 Cable Failure Time

Description

Even though an electrical cable is considered a “target”, the cable failure time quantity is included in this study to assess the models’ ability to predict the time to cable failure. This is an indirect way of assessing the model prediction of temperature. The model only predicts the interior temperature of the cable, and the failure time is considered as the time at which the predicted temperature rises above an experimentally determined value.

The thermally-induced electrical failure (THIEF) of a cable can be predicted via a simple one-dimensional heat transfer calculation, under the assumption that the cable can be treated as a homogeneous cylinder [7]. The governing equation for the cable temperature, $T(r,t)$ (°C), is given by

$$\rho c \left(\frac{\partial T}{\partial t} \right) = \frac{1}{r} \frac{\partial}{\partial r} k r \left(\frac{\partial T}{\partial r} \right) \quad (5.1)$$

where ρ , c and k are the effective density (kg/m^3), specific heat ($\text{J}/(\text{g} \cdot \text{K})$), and thermal conductivity ($\text{W}/\text{m} \cdot \text{K}$) of the solid, respectively, and r is the radius of the cable (m). The boundary condition at the exterior boundary, $r = R$, is defined as

$$\dot{q}'' = k \left(\frac{\partial T}{\partial r} \right) (R, t) \quad (5.2)$$

where \dot{q}'' is the assumed axially-symmetric heat flux to the exterior surface of the cable (kW/m^2). The net heat flux at the surface of the cable is determined from the exposing gas temperature surrounding the cable at the n -th time step, $T_g(t^n)$

$$\dot{q}''(t^n) = \varepsilon \sigma (T_g(t^n)^4 - (T_s^n)^4) + h(T_g(t^n) - T_s^n) \quad (5.3)$$

where ε is the emissivity of the cable surface (assumed to be 0.95), σ is the Stefan-Boltzmann constant ($5.67 \times 10^{-8} \text{ W}/(\text{m}^2 \cdot \text{K}^4)$), h is the convective heat transfer coefficient (assumed to be $10 \text{ W}/(\text{m}^2 \cdot \text{K})$, which is typical of free convection), $T_g(t^n)$ is the effective gas temperature at the n -th time step (K), and T_s^n is the surface temperature of the cable (K).

A slight complication of the solution methodology described above is in situations where the cable is surrounded by a protective layer like a conduit, armor jacket, or tray covering. In CAROLFIRE, only conduits were considered in the modeling, but other protective measures can be handled in similar fashion, assuming test data is available to validate the various physical assumptions.

A conduit forms a thermal barrier between the hot gases of a fire and the cable itself. A simple way to incorporate its effect into the THIEF model is to replace the “exposing” gas temperature, T_g , in Eq. 5.3 by the conduit’s temperature, T_c . In other words, the cable no longer “sees” the hot gases from the fire, but rather the interior surface of the conduit.

A steel conduit may be assumed to exhibit thermally-thin behavior; that is, its conductivity is so large that for all practical purposes it can be assumed that its exterior and interior surface temperatures are equal. Its temperature increases due to the heat flux from the hot gases at its exterior surface, which is given by

$$\dot{q}_{\text{ext}}''(t^n) = \varepsilon_c \sigma (T_g(t^n)^4 - (T_c^n)^4) + h(T_g(t^n) - T_c^n) \quad (5.4)$$

where T_c^n is the conduit temperature at the n -th time step (K), and ε_c is the emissivity of its surface (assumed to be 0.85, which is typical of non-polished steel). Heat is transferred from the interior surface of the conduit to the cable surface via radiation and convection

$$\dot{q}_{\text{int}}''(t^n) = F \sigma ((T_c^n)^4 - (T_s^n)^4) + h(T_c^n - T_s^n) \quad (5.5)$$

where

$$F = \left(\left(\frac{R_c}{R} \right) \frac{1}{\varepsilon} + \frac{1 - \varepsilon_c}{\varepsilon_c} \right)^{-1} \quad (5.6)$$

where R_c is the inner radius of the conduit (m). The view factor, F , was based on the assumption that the conduit and cable are concentric cylinders [7].

Verification

This example case is based on Penlight Test 7 from the Cable Response to Live Fire (CAROLFIRE) [7] series. This test involved a cable inside of conduit that was located in a heated cylindrical enclosure.

Table 5.1: Verification case, cable failure time.

User-Specified Input	
Parameter	Value
Time Ramp	0, 80, 820, 1240, 1800, 1900
Temperature Ramp	24, 460, 460, 460, 460, 0
Cable Diameter (mm)	16.3
Mass per Unit Length (kg/m)	0.529
Jacket Thickness (mm)	1.5
Conduit Diameter (mm)	50
Conduit Thickness (mm)	4.9
T_{∞} (°C)	24

Calculated Output			
Time (s)	Exposing Temperature (°C)	Cable Temperature (°C)	Conduit Temperature (°C)
0	24.0	24.0	24.0
24	155.0	24.0	25.6
50	296.3	24.1	32.4
80	460.0	24.6	52.3
130	460.0	27.5	98.7
240	460.0	44.7	186.9
370	460.0	81.5	265.9
500	460.0	130.5	320.6
740	460.0	227.3	379.1
900	460.0	282.8	401.3
1140	460.0	345.8	422.8
1300	460.0	375.9	432.5
1460	460.0	398.4	439.8
1473	460.0	400.0	440.3
1800	460.0	428.6	449.6

Validation

A summary of the comparisons between predicted and measured cable failure times (the time at which the cable reaches its threshold failure temperature, which corresponds to 200 °C for thermoplastic cables and 400 °C for thermoset cables) is shown in Fig. 5.1.

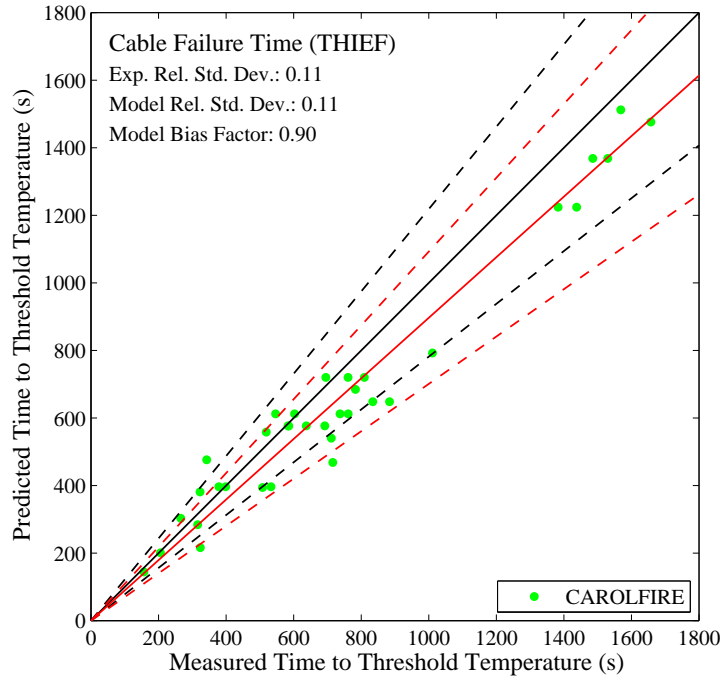


Figure 5.1: Summary of cable failure time predictions.

5.2 Unprotected Steel Temperature

Description

The temperature rise, ΔT_s ($^{\circ}\text{C}$), of an unprotected steel member exposed to fire can be predicted using [33]

$$\Delta T_s = \frac{F}{V} \frac{1}{\rho_s c_s} [h_c(T_f - T_s) + \sigma \varepsilon(T_f^4 - T_s^4)] \Delta t \quad (5.7)$$

where F/V is the ratio of heated surface area to volume (m^{-1}), ρ_s is the density of steel (kg/m^3), c_s is the specific heat of steel ($\text{J}/(\text{kg} \cdot \text{K})$), h_c is the convective heat transfer coefficient ($\text{W}/(\text{m}^2 \cdot \text{K})$), T_f is the exposing fire temperature (K), T_s is the steel temperature (K), σ is the Stefan-Boltzmann constant ($\text{W}/(\text{m}^2 \cdot \text{K}^4)$), ε is the flame emissivity, and Δt is the time step (s). Note that the HGL temperature, plume temperature, or other exposing temperature can be used as the fire temperature, T_f .

Verification

This example case is based on the 1.1 m Diesel Fire Test from the SP AST Column [16] series. This test involved a large test hall with a steel column located in the middle of a diesel pool fire.

Note: In this verification case, the McCaffrey method (see Section 4.2) is used to calculate the exposing fire temperature, T_f .

Table 5.2: Verification case, unprotected steel temperature.

User-Specified Input	
Parameter	Value
F/V (1/m)	205
ρ_s (kg/m ³)	7833
c_s (kJ/(kg · K))	0
ε	0
h_c (W/(m ² · K))	25
Correlation for T_f	McCaffrey
\dot{Q} (kW)	1434
Height (m)	1
T_∞ (°C)	20

Calculated Output		
Time (s)	Fire Temperature (°C)	Steel Temperature (°C)
0	872.81	20.0
15	872.81	89.7
30	872.81	162.4
45	872.81	232.8
60	872.81	300.6
120	872.81	536.6
180	872.81	700.6
240	872.81	793.6
300	872.81	838.7
600	872.81	872.4
900	872.81	872.8
1200	872.81	872.8
1500	872.81	872.8

5.3 Protected Steel Temperature

Description

The temperature rise, ΔT_s ($^{\circ}\text{C}$), of a protected steel member exposed to fire can be predicted, but we must first determine if the thermal capacity of the insulation layer should be accounted for or if it can be neglected [33].

$$\Delta T_s = \begin{cases} k_i \left(\frac{T_f - T_s}{c_s h \frac{W}{D}} \right) \Delta t & c_s \frac{W}{D} > 2c_i \rho_i h \\ \frac{k_i}{h} \left(\frac{T_f - T_s}{c_s \frac{W}{D} + \frac{1}{2} c_i \rho_i h} \right) \Delta t & c_s \frac{W}{D} < 2c_i \rho_i h \end{cases} \quad (5.8)$$

where k_i is the thermal conductivity of the insulation material ($\text{W}/(\text{m} \cdot \text{K})$), T_f is the exposing fire temperature (K), T_s is the steel temperature (K), c_s is the specific heat of steel ($\text{J}/(\text{kg} \cdot \text{K})$), c_i is the specific heat of the insulation material ($\text{J}/(\text{kg} \cdot \text{K})$), h is the thickness of the insulation (m), W/D is the ratio of the weight of steel section per unit length to the heated perimeter (kg/m^2), ρ_i is the density of the insulating material (kg/m^3), and Δt is the time step (s). Note that the HGL temperature, plume temperature, or other exposing temperature can be used as the fire temperature, T_f .

Verification

This example case examines the temperature of a bar structural element in Test 4 of the World Trade Center (WTC) [23] series. This test involved a simple compartment with a heptane spray burner and various structural elements with varying amounts of sprayed fire-resistive materials.

Note: In this verification case, the MQH method (see Section 2.1) is used to calculate the exposing fire temperature, T_f .

Table 5.3: Verification case, protected steel temperature.

User-Specified Input	
Parameter	Value
c_s (kJ/(kg · K))	0.450
W/D (kg/m ²)	50.1
k_i (W/(m · K))	0.10
ρ_i (kg/m ³)	208
c_i (kJ/(kg · K))	2.0
h_i (m)	0.0191
Correlation for T_f	MQH
\dot{Q} (kW)	3200
L (m)	7.04
W (m)	3.60
H (m)	3.82
H_o (m)	2.82
W_o (m)	2.4
k (kW/(m · K))	0.00012
ρ (kg/m ³)	737
c (kJ/(kg · K))	1.42
δ (m)	0.0254
T_∞ (°C)	20

Table 5.4: Verification case, protected steel temperature (continued).

Calculated Output		
Time (s)	Fire Temperature (°C)	Steel Temperature (°C)
0	25.9	20.00
50	378.7	24.14
100	422.6	29.24
200	471.9	40.51
300	503.5	52.54
400	527.3	65.00
500	546.5	77.72
600	562.7	90.60
700	576.9	103.56
800	589.4	116.55
840	594	121.74

Validation

For the unprotected and protected steel cases, a summary of the comparisons between peak predicted and measured target temperatures is shown in Fig. 5.2.

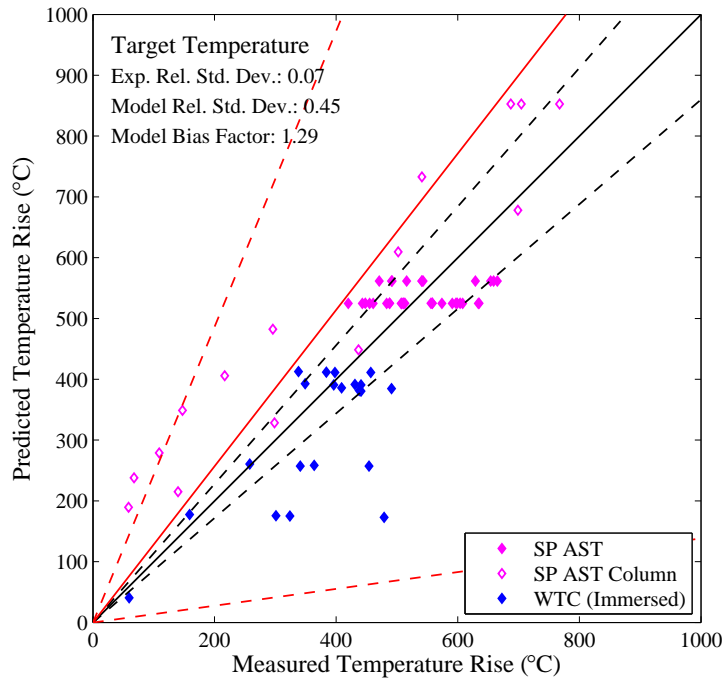


Figure 5.2: Summary of target temperature predictions.

Chapter 6

Target Heat Flux

Thermal radiation is an important mode of heat transfer in fires. The empirical correlations include simple estimates of flame radiation from a point or cylindrical source.

6.1 Point Source Radiation Heat Flux

Description

The point source model assumes that radiative energy is concentrated at a point located within a flame [34]. Here, the point source is located at a point one-third the height of the flame. The radiative heat flux, \dot{q}_r'' (kW/m²), at any distance R (m) from this point can be predicted using

$$\dot{q}_r'' = \cos \theta \left(\frac{\chi_r \dot{Q}}{4\pi R^2} \right) \quad (6.1)$$

where the $\cos \theta$ term (equal to x/R for targets facing sideways, or z/R for gauges facing upward or downward) accounts for a target that is at an angle θ from the source. In the Fortan implementation of this empirical correlation, the IOR orientation parameter is used to specify which direction the target or gauge is facing: 1 or -1 for the positive or negative x direction, 2 or -2 for the positive or negative y direction, and 3 or -3 for the positive or negative z direction. In Eq. 6.1, χ_r is the radiative fraction (unless provided in the test report, a value of 0.35 was used), \dot{Q} is the HRR of the fire (kW), and R is the radial distance from the point source to the edge of the target (m) and is given by

$$R = \sqrt{x^2 + \left(z - \frac{L_f}{3}\right)^2} \quad (6.2)$$

where x is the horizontal distance from the point source to the edge of the target (m), and z is the height of the heat flux target (m). The flame height, L_f (m), is given by

$$L_f = D(3.7Q^{*2/5} - 1.02) \quad (6.3)$$

where D is the diameter of the fire source (m) and is given by

$$D = \sqrt{\frac{4A}{\pi}} \quad (6.4)$$

where A is the area of the fire source (m²). The nondimensional HRR, Q^* , is given by

$$Q^* = \frac{\dot{Q}}{\rho_\infty c_p T_\infty \sqrt{g} D^{5/2}} \quad (6.5)$$

where ρ_∞ is the ambient air density (kg/m^3), c_p is the specific heat of air ($\text{kJ}/(\text{kg} \cdot \text{K})$), T_∞ is the ambient air temperature (K), and g is the acceleration of gravity (m/s^2).

Verification

This example case is based on Test 7 from the Fleury Heat Flux [8] series. This test involved a 100 kW propane burner with dimensions of 0.3 m by 0.3 m and heat flux measurements at various distances from the burner.

Table 6.1: Verification case, point source radiation heat flux.

User-Specified Input	
Parameter	Value
\dot{Q} (kW)	100
χ_r	0.35
A (m^2)	0.09
x (m)	0.50, 0.75, 1.0
z (m)	0.0
IOR	2

Calculated Output	
Radius (m)	Heat Flux (kW/m^2)
0.50	6.01
0.75	3.65
1.00	2.33

Validation

A summary of the comparisons between peak predicted and measured heat fluxes is shown in Fig. 6.1.

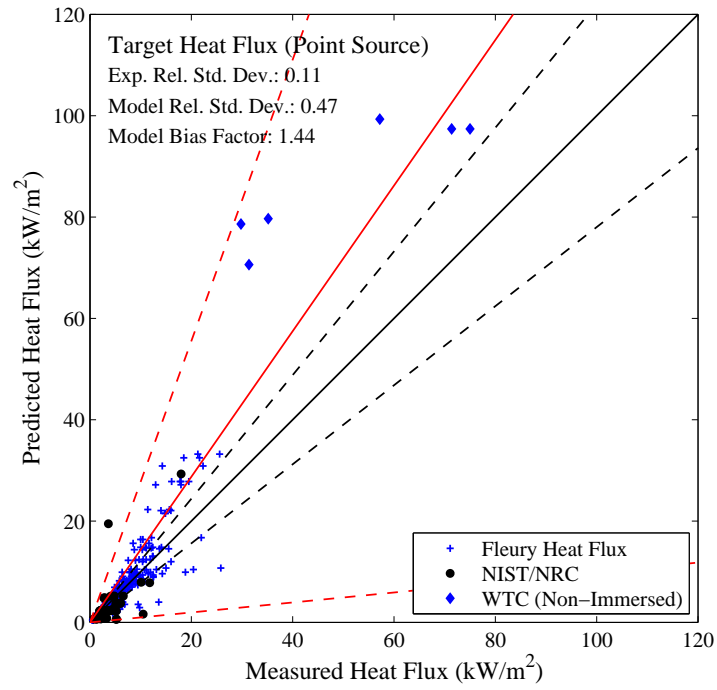


Figure 6.1: Summary of point source radiation heat flux predictions.

6.2 Solid Flame Radiation Heat Flux

Description

The solid flame model predicts the heat flux to a target based on the effective emissive power from a flame and a view factor calculation [34]. The radiative heat flux, \dot{q}_r'' (kW/m²), at any distance R (m) from the center of the flame can be predicted using

$$\dot{q}_r'' = EF_{12} \quad (6.6)$$

where E is the effective emissive power of the flame (kW/m²), and F_{12} is the view factor between the target and the flame. The effective emissive power of the flame, E , is given by

$$E = 58(10^{-0.0823D}) \quad (6.7)$$

where D is the effective fire diameter (m).

Ground-Level Target

For a heat flux target that is at the same level as the base of the flame, the view factor between the target and the flame, F_{12} , is given by

$$F_{12} = \sqrt{F_{12,H}^2 + F_{12,V}^2} \quad (6.8)$$

where $F_{12,H}$ and $F_{12,V}$ are given by

$$F_{12,H} = \frac{(B - \frac{1}{S})}{\pi\sqrt{B^2 - 1}} \tan^{-1} \sqrt{\frac{(B+1)(S-1)}{(B-1)(S+1)}} - \frac{(A - \frac{1}{S})}{\pi\sqrt{A^2 - 1}} \tan^{-1} \sqrt{\frac{(A+1)(S-1)}{(A-1)(S+1)}} \quad (6.9)$$

$$F_{12,V} = \frac{1}{\pi S} \tan^{-1} \left(\frac{H}{\sqrt{S^2 - 1}} \right) - \frac{H}{\pi S} \tan^{-1} \sqrt{\frac{S-1}{S+1}} + \frac{AH}{\pi S\sqrt{A^2 - 1}} \tan^{-1} \sqrt{\frac{(A+1)(S-1)}{(A-1)(S+1)}} \quad (6.10)$$

where H , S , A , and B are given by

$$H = \frac{2L_f}{D} \quad (6.11)$$

$$S = \frac{2x}{D} \quad (6.12)$$

$$A = \frac{H^2 + S^2 + 1}{2S} \quad (6.13)$$

$$B = \frac{1 + S^2}{2S} \quad (6.14)$$

where x is the horizontal distance from the center of the flame to the edge of the heat flux target (m), and L_f is the flame height given in Eq. 6.3 (m).

Elevated Target

For a heat flux target that is elevated from the base of the flame, the view factor between the target and the flame, F_{12} , is given by

$$F_{12} = F_{12,v1} + F_{12,v2} \quad (6.15)$$

where $F_{12,v1}$ and $F_{12,v2}$ are given by

$$F_{12,v1} = \frac{1}{\pi S} \tan^{-1} \left(\frac{H_1}{\sqrt{S^2 - 1}} \right) - \frac{H_1}{\pi S} \tan^{-1} \sqrt{\frac{S-1}{S+1}} + \frac{A_1 H_1}{\pi S \sqrt{A_1^2 - 1}} \tan^{-1} \sqrt{\frac{(A_1 + 1)(S-1)}{(A_1 - 1)(S+1)}} \quad (6.16)$$

$$F_{12,v2} = \frac{1}{\pi S} \tan^{-1} \left(\frac{H_2}{\sqrt{S^2 - 1}} \right) - \frac{H_2}{\pi S} \tan^{-1} \sqrt{\frac{S-1}{S+1}} + \frac{A_2 H_2}{\pi S \sqrt{A_2^2 - 1}} \tan^{-1} \sqrt{\frac{(A_2 + 1)(S-1)}{(A_2 - 1)(S+1)}} \quad (6.17)$$

where H_1 , H_2 , S , A_1 , and A_2 are given by

$$H_1 = \frac{2z}{D} \quad (6.18)$$

$$H_2 = \frac{2(L_f - z)}{D} \quad (6.19)$$

$$S = \frac{2x}{D} \quad (6.20)$$

$$A_1 = \frac{H_1^2 + S^2 + 1}{2S} \quad (6.21)$$

$$A_2 = \frac{H_2^2 + S^2 + 1}{2S} \quad (6.22)$$

where x is the horizontal distance from the center of the flame to the edge of the heat flux target (m), z is the height of the target from the base of the flame (m), and L_f is the flame height given in Eq. 6.3 (m).

Verification

This example case is based on Test 7 from the Fleury Heat Flux [8] series. This test involved a 100 kW propane burner with dimensions of 0.3 m by 0.3 m and heat flux measurements at various distances from the burner.

Table 6.2: Verification case, solid flame radiation heat flux.

User-Specified Input	
Parameter	Value
\dot{Q} (kW)	100
A (m ²)	0.09
x (m)	0.50, 0.75, 1.0
z (m)	0.0

Calculated Output	
Radius (m)	Heat Flux (kW/m ²)
0.50	11.18
0.75	6.90
1.00	4.69

Validation

A summary of the comparisons between peak predicted and measured plume temperatures is shown in Fig. 6.2.

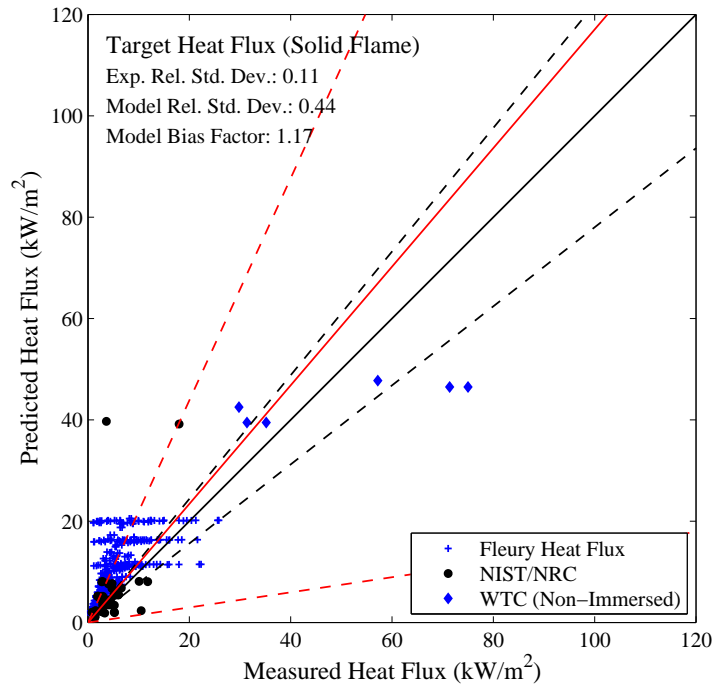


Figure 6.2: Summary of solid flame radiation heat flux predictions.

Chapter 7

Ceiling Jet Temperature

The ceiling jet is the shallow layer of hot gases below the ceiling that spreads radially from the centerline of the fire plume. The ceiling jet has a higher temperature than the overall temperature of the HGL, and therefore it is important where targets are located just below the ceiling.

Description

For a steady-state fire, the correlation of Alpert [35] predicts that the ceiling jet temperature rise, ΔT_{jet} ($^{\circ}\text{C}$), from a fire plume is given by

$$\Delta T_{\text{jet}} = \begin{cases} \frac{16.9\dot{Q}^{2/3}}{H^{5/3}} & r/H \leq 0.18 \\ \frac{5.38(\dot{Q}/r)^{2/3}}{H} & r/H > 0.18 \end{cases} \quad (7.1)$$

where \dot{Q} is the total HRR (kW), H is the height of the ceiling above the fuel (m), and r is the radial distance to the detector (m).

Note that some of these cases assume a quasi-steady approach for a fire source \dot{Q} that follows a specified t -squared growth rate, which is given by

$$\dot{Q} = \alpha t^2 \quad (7.2)$$

where α is the t -squared growth rate parameter (kW/s²), and t is time (s).

For cases in which the fire was located against a wall or corner, these correlations are adjusted based on the method of reflection. For a fire adjacent to a flat wall, $2\dot{Q}$ is substituted for \dot{Q} ; and for a fire in a 90-degree corner, $4\dot{Q}$ is substituted for \dot{Q} . This adjustment is denoted in the input parameters as the location factor. For a given case, the location factor has a value of 1, 2, or 4, which corresponds to a fire away from walls or corners, a fire adjacent to a wall, or a fire located in a corner, respectively.

Verification

This example case is based on Test 1 from the NIST and Nuclear Regulatory Commission (NIST/NRC) [13] series. This test involved a compartment with a closed door, a heptane spray burner, and no ventilation.

Table 7.1: Verification case, ceiling jet temperature.

User-Specified Input	
Parameter	Value
\dot{Q} (kW)	410
Location Factor	1
r (m)	5.90
H (m)	3.72
T_{∞} (°C)	22

Calculated Output
Ceiling Jet Temperature (°C)
46.45

Validation

A summary of the comparisons between peak predicted and measured ceiling jet temperatures is shown in Fig. 7.1.

It is important to note that this ceiling jet temperature correlation was developed using data from tests that were conducted in a large facility in which the distant walls and large compartment size did not allow for the development of a significant hot gas layer. In a more typical fire scenario (i.e., a smaller compartment), the HGL develops relatively quickly, and temperatures at the ceiling are affected by the ceiling jet as well as the accumulating HGL. Thus, when compared to experimentally measured ceiling temperatures in a compartment fire, this correlation tends to underpredict the temperatures because it is not accounting for the development of the HGL. This is an important consideration when using this correlation to predict detector or sprinkler activations.

For the reasons stated above, two scatter plot comparisons are shown in Fig. 7.1. One scatter plot shows the results for unconfined tests that were conducted under a false ceiling in which the hot plume gases did not accumulate to form an HGL, but were allowed to spill out from under a false ceiling. The other scatter plot shows the results of underpredicted temperature comparisons for compartment fire tests. The use of the ceiling jet correlation in a confined compartment with the presence of an HGL can result in an underprediction of the measured ceiling jet temperature by approximately 70 %. Therefore, the model bias factor and model relative standard deviation were only calculated for the unconfined ceiling jet cases that the correlation was developed for. In the unconfined ceiling cases, the ceiling temperature predictions are in better agreement with experimental data because this scenario is more representative of a temperature rise due to only ceiling jet flow from the fire plume.

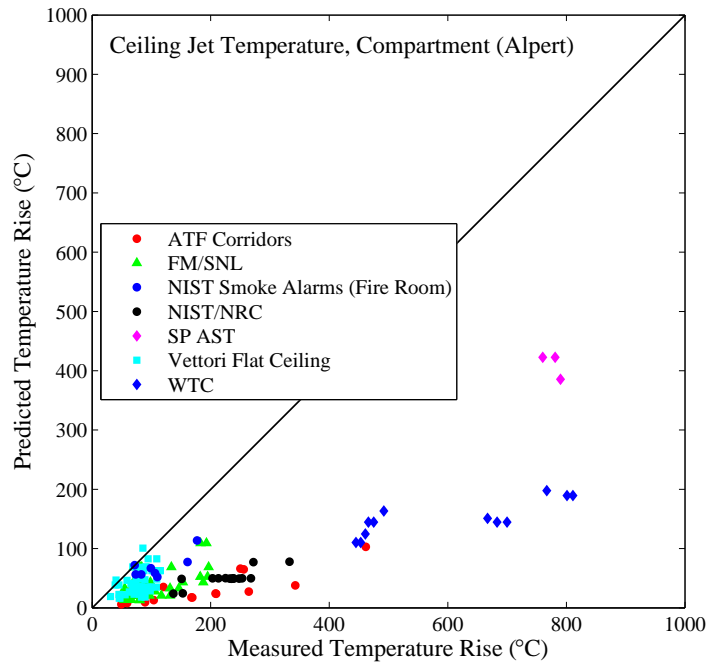
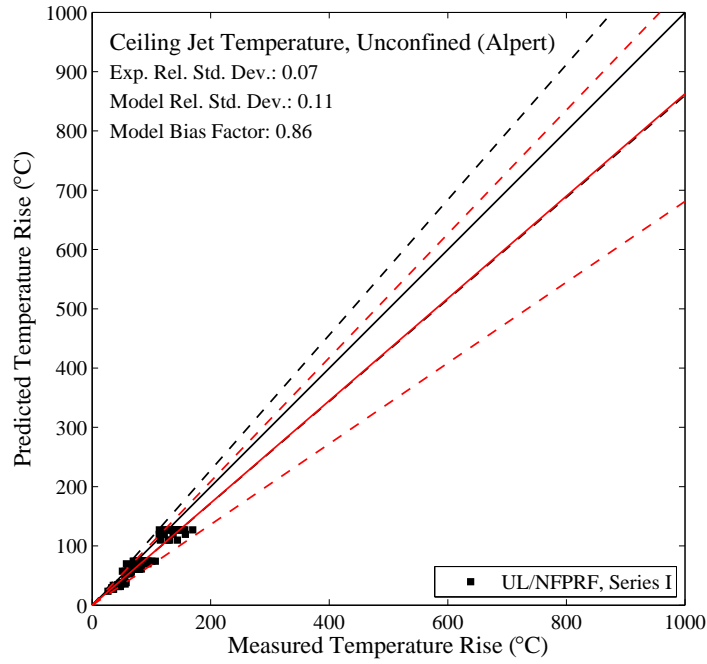


Figure 7.1: Summary of compartment (top) and unconfined (bottom) ceiling jet temperature predictions.

Chapter 8

Sprinkler Activation Time

Much like an electrical cable, a sprinkler is merely a “target” with a particular set of thermal properties, such as the response time index (RTI) that indicates the sensitivity of the fusible link or glass bulb. Activation is assumed to occur when the link or bulb temperatures reaches a predetermined threshold temperature.

Description

For a steady-state fire, the correlation of Alpert [35] predicts that the activation time of a sprinkler, t_{act} (s), is given by [36]

$$t_{act} = \frac{RTI}{\sqrt{u_{jet}}} \ln \left(\frac{T_{jet} - T_{\infty}}{T_{jet} - T_{act}} \right) \quad (8.1)$$

where RTI is the response time index of the sprinkler ($(m \cdot s)^{1/2}$), T_{∞} is the ambient air temperature ($^{\circ}C$), and T_{act} is the activation temperature of the sprinkler ($^{\circ}C$). The ceiling jet temperature, T_{jet} ($^{\circ}C$), is given by

$$T_{jet} = \begin{cases} \frac{16.9\dot{Q}^{2/3}}{H^{5/3}} + T_{\infty} & r/H \leq 0.18 \\ \frac{5.38(\dot{Q}/r)^{2/3}}{H} + T_{\infty} & r/H > 0.18 \end{cases} \quad (8.2)$$

where \dot{Q} is the total HRR (kW), H is the height of the ceiling above the fuel (m), and r is the radial distance to the detector (m). The ceiling jet velocity, u_{jet} (m/s), is given by

$$u_{jet} = \begin{cases} 0.947 \left(\frac{\dot{Q}}{H} \right)^{1/3} & r/H \leq 0.15 \\ \frac{0.197\dot{Q}^{1/3}H^{1/2}}{r^{5/6}} & r/H > 0.15 \end{cases} \quad (8.3)$$

Note that some of these cases assume a quasi-steady approach for a fire source \dot{Q} that follows a specified t -squared growth rate, which is given by Eq. 7.2.

For cases in which the fire was located against a wall or corner, these correlations are adjusted based on the method of reflection. For a fire adjacent to a flat wall, $2\dot{Q}$ is substituted for \dot{Q} ; and for a fire in a 90-degree corner, $4\dot{Q}$ is substituted for \dot{Q} [35]. This adjustment is denoted in the input parameters as the location factor. For a given case, the location factor has a value of 1, 2, or 4, which corresponds to a fire away from walls or corners, a fire adjacent to a wall, or a fire located in a corner, respectively.

Verification

This example case is based on Test 1 from the Vettori Flat Ceiling [21] series. This test involved residential quick response sprinklers located on a flat ceiling in a compartment with a closed door, a methane burner, and no ventilation.

Table 8.1: Verification case, sprinkler activation time.

User-Specified Input	
Parameter	Value
α (kW/s ²)	0.105
Location Factor	1
RTI ((m · s) ^{1/2})	55
T_{act} (°C)	68
r (m)	2.20
H (m)	2.09
T_{∞} (°C)	16.6

Calculated Output		
Time (s)	HRR (kW)	Activation Time (s)
50	262.5	98.2

Validation

A summary of the comparisons between predicted and measured sprinkler activation times is shown in Fig. 8.1.

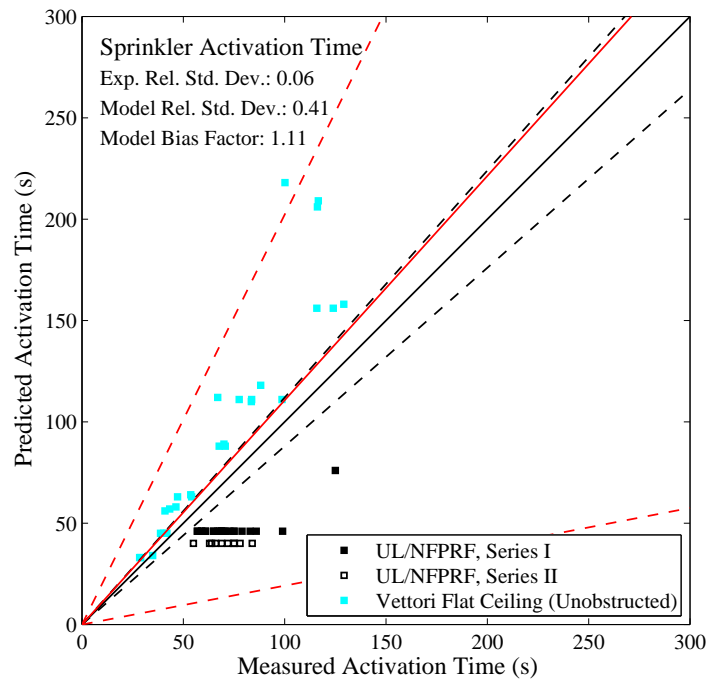


Figure 8.1: Summary of sprinkler activation time predictions.

Chapter 9

Smoke Detector Activation Time

Smoke detector activation can be modeled in a variety of ways. A common method is to assume that the detector behaves like a very sensitive sprinkler with a low activation temperature and RTI.

Description

For this method, the prediction of smoke detector activation time is identical to that for a sprinkler (as described in Chapter 8). Equations 8.1, 8.2, and 8.3 are used to calculate the time at which the detector reaches its activation temperature, and the input parameters are the same as described in Chapter 8. Bukowski and Averill [37] suggested an activation temperature that corresponds to a temperature rise above ambient, ΔT_c , of 5 °C to be typical of many residential smoke alarms. It is assumed that the smoke detectors are low-RTI devices ($RTI = 5 \text{ (m} \cdot \text{s)}^{1/2}$).

Note that some of these cases assume a quasi-steady approach for a fire source \dot{Q} that follows a specified t -squared growth rate, which was specified as $\dot{Q} = \alpha t^2$ up to a cutoff time of t_{fire} . In this approach, for a given time and HRR, Eq. 8.1 was used to calculate the time that the detector would activate. If the calculated activation time was less than the current time, then the detector was assumed to activate. After the time t_{fire} , the fire HRR was steady.

Verification

This example case is based on Test SDC02 from the NIST Smoke Alarms [14] series. This test involved ionization and photoelectric smoke alarms located in a single-story manufactured home with a closed door, an upholstered chair fuel source, and no ventilation. If the fire size is not sufficiently large enough to activate the detector, then the activation time is denoted as not applicable (N/A).

Table 9.1: Verification case, smoke detector activation time.

User-Specified Input	
Parameter	Value
α (kW/s ²)	0.00463
Location Factor	1
RTI ((m · s) ^{1/2})	5
ΔT_c (°C)	5
r (m)	1.3
H (m)	2.1
t_{fire} (s)	300
T_∞ (°C)	21

Calculated Output		
Time (s)	HRR (kW)	Activation Time (s)
25	2.90	N/A
26	3.10	N/A
27	3.40	N/A
28	3.63	35.0
29	3.89	23.3

Validation

A summary of the comparisons between predicted and measured smoke detector activation times is shown in Fig. 9.1.

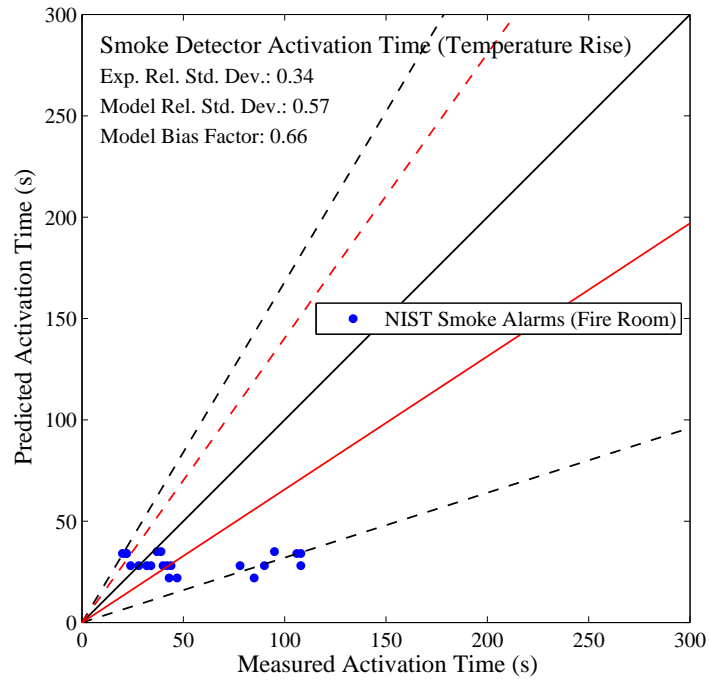


Figure 9.1: Summary of smoke detector activation time predictions using the Temperature Rise method.

Chapter 10

Summary

Summary of Uncertainty Statistics for Empirical Correlations

For each quantity of interest, the experimental relative standard deviation, $\tilde{\sigma}_E$, model relative standard deviation, $\tilde{\sigma}_M$, and model bias factor are shown in Table 10.1, which are taken from each of the scatter plots in the corresponding chapters of this document. The latter two values indicate the average scatter and bias of the model predictions. For example, for a given quantity, a model relative standard deviation of 0.15 indicates that one standard deviation of all of the model predictions is equal to 15 %, and a model bias factor of 1.05 indicates that, on average, the model tends to overpredict that quantity by 5 %. The number of datasets and data points are also listed for each quantity.

For quantities with only a small number of experimental data points, additional experimental data is needed to justify the model uncertainty and bias. Note that some quantities exhibit a large amount of model uncertainty or are significantly under- or over-predicted, and some caution should be exercised when applying these empirical correlations. More detailed discussion on the application and usage of these statistical metrics is provided in the “Quantifying Model Uncertainty” chapter of the FDS Validation Guide [5].

Table 10.1: Summary statistics for all quantities of interest

Quantity	Section	Datasets	Points	$\tilde{\sigma}_E$	$\tilde{\sigma}_M$	Bias
HGL Temperature, Natural Ventilation (MQH)	2.1	5	78	0.07	0.15	1.17
HGL Temperature, Forced Ventilation (FPA)	2.2	3	66	0.07	0.32	1.29
HGL Temperature, Forced Ventilation (DB)	2.3	3	66	0.07	0.25	1.18
HGL Temperature, No Ventilation (Beyler)	2.4	2	18	0.07	0.37	1.04
Plume Temperature (Heskestad)	4.1	5	156	0.07	0.33	0.84
Plume Temperature (McCaffrey)	4.2	5	162	0.07	0.31	0.90
Cable Failure Time (THIEF)	5.1	1	35	0.11	0.11	0.90
Target Temperature	5.2	3	72	0.07	0.45	1.29
Target Heat Flux (Point Source)	6.1	3	658	0.11	0.47	1.44
Target Heat Flux (Solid Flame)	6.2	3	658	0.11	0.44	1.17
Ceiling Jet Temperature, Unconfined (Alpert)	7.1	1	103	0.07	0.11	0.86
Sprinkler Activation Time	8.1	3	60	0.06	0.41	1.11
Smoke Detector Activation Time (Temperature Rise)	9.1	1	24	0.34	0.57	0.66

Bibliography

- [1] K. Hill, J. Dreisbach, F. Joglar, B. Najafi, K. McGrattan, R. Peacock, and A. Hamins. Verification and Validation of Selected Fire Models for Nuclear Power Plant Applications. NUREG-1824, United States Nuclear Regulatory Commission, Washington, DC, 2007. [iii](#)
- [2] D. Stroup and A. Lindeman. Verification and Validation of Selected Fire Models for Nuclear Power Plant Applications. NUREG-1824, supplement 1, United States Nuclear Regulatory Commission, Washington, DC, 2013. [iii](#), [1](#)
- [3] R. D. Peacock, G. P. Forney, and P. A. Reneke. CFAST – Consolidated Model of Fire Growth and Smoke Transport (Version 6): Technical Reference Guide. Special Publication 1026, National Institute of Standards and Technology, Gaithersburg, Maryland, July 2011. [1](#)
- [4] K. McGrattan, S. Hostikka, R. McDermott, J. Floyd, C. Weinschenk, and K. Overholt. *Fire Dynamics Simulator, Technical Reference Guide, Volume 2: Verification*. National Institute of Standards and Technology, Gaithersburg, Maryland, USA, and VTT Technical Research Centre of Finland, Espoo, Finland, sixth edition, September 2013. [1](#)
- [5] K. McGrattan, S. Hostikka, R. McDermott, J. Floyd, C. Weinschenk, and K. Overholt. *Fire Dynamics Simulator, Technical Reference Guide, Volume 3: Validation*. National Institute of Standards and Technology, Gaithersburg, Maryland, USA, and VTT Technical Research Centre of Finland, Espoo, Finland, sixth edition, September 2013. [1](#), [2](#), [6](#), [59](#)
- [6] D.T. Sheppard and B.W. Klein. Burn Tests in Two Story Structure with Hallways. Technical report, ATF Laboratories, Ammdendale, Maryland, 2009. [2](#), [65](#)
- [7] S.P. Nowlen, F.J. Wyant, and K.B. McGrattan. Cable Response to Live Fire (CAROLFIRE). NUREG/CR 6931, United States Nuclear Regulatory Commission, Washington, DC, April 2008. [2](#), [29](#), [30](#), [31](#), [66](#), [67](#), [68](#)
- [8] R. Fleury. Evaluation of Thermal Radiation Models for Fire Spread Between Objects. Master's thesis, University of Canterbury, Christchurch, New Zealand, 2010. [2](#), [40](#), [44](#), [69](#)
- [9] S.P. Nowlen. Enclosure Environment Characterization Testing for the Baseline Validation of Computer Fire Simulation Codes. NUREG/CR-4681 (SAND86-1296), Sandia National Laboratory, Albuquerque, New Mexico, March 1987. Work performed under contract to the US Nuclear Regulatory Agency, Washington DC. [2](#), [8](#), [11](#), [70](#), [71](#), [72](#)
- [10] J.M. Chavez and S.P. Nowlen. An Experimental Investigation of Internally Ignited Fires in Nuclear Power Plant Control Cabinets, Part II: Room Effects Tests. NUREG/CR-4527 (SAND86-0336), Sandia National Laboratory, Albuquerque, New Mexico, November 1988. Work performed under contract to the US Nuclear Regulatory Agency, Washington DC. [2](#), [8](#), [11](#), [70](#), [71](#), [72](#)

- [11] K.L. Foote. 1986 LLNL Enclosure Fire Tests Data Report. Technical Report UCID-21236, Lawrence Livermore National Laboratory, August 1987. [2](#), [4](#), [14](#), [74](#)
- [12] R.D. Peacock, S. Davis, and W.T. Lee. An Experimental Data Set for the Accuracy Assessment of Room Fire Models. NBSIR 88-3752, National Bureau of Standards (now NIST), Gaithersburg, Maryland, April 1988. [2](#), [76](#)
- [13] A. Hamins, A. Maranghides, R. Johnsson, M. Donnelly, G. Yang, G. Mulholland, and R.L. Anleitner. Report of Experimental Results for the International Fire Model Benchmarking and Validation Exercise 3. NIST Special Publication 1013-1, National Institute of Standards and Technology, Gaithersburg, Maryland, May 2006. Joint Publication of NIST and the US Nuclear Regulatory Commission (NUREG/CR-6905). [2](#), [18](#), [21](#), [48](#), [77](#), [78](#), [79](#)
- [14] R.W. Bukowski, R.D. Peacock, J.D. Averill, T.G. Cleary, N.P. Bryner, W.D. Walton, P.A. Reneke, and E.D. Kuligowski. Performance of Home Smoke Alarms Analysis of the Response of Several Available Technologies in Residential Fire Settings. NIST Technical Note 1455-1, National Institute of Standards and Technology, Gaithersburg, Maryland, February 2008. [2](#), [56](#), [80](#), [81](#)
- [15] U. Wickström, R. Jansson, and H. Tuovinen. Verification fire tests on using the adiabatic surface temperature for predicting heat transfer. Technical Report 2009:19, SP Technical Research Institute of Sweden, Båras, Sweden, 2009. [2](#), [83](#), [84](#)
- [16] J. Sjöström, A. Byström, and U. Wickström. Large scale test on thermal exposure to steel column exposed to pool fires. Technical Report 2012:04, SP Technical Research Institute of Sweden, Båras, Sweden, 2012. ISBN: 978-91-87017-21-6. [2](#), [34](#), [85](#), [86](#)
- [17] K.D. Steckler, J.G. Quintiere, and W.J. Rinkinen. Flow Induced By Fire in A Compartment. NBSIR 82-2520, National Bureau of Standards (now NIST), Gaithersburg, Maryland, September 1982. [2](#), [87](#)
- [18] D.T. Sheppard and D.R. Steppan. Sprinkler, Heat & Smoke Vent, Draft Curtain Project – Phase 1 Scoping Tests. Technical report, Underwriters Laboratories, Northbrook, Illinois, May 1997. [2](#), [89](#), [90](#)
- [19] K.B. McGrattan, A. Hamins, and D. Stroup. Sprinkler, Smoke & Heat Vent, Draft Curtain Interaction — Large Scale Experiments and Model Development. NISTIR 6196-1, National Institute of Standards and Technology, Gaithersburg, Maryland, September 1998. [2](#), [89](#), [90](#)
- [20] J.E. Gott, D.L. Lowe, K.A. Notarianni, and W.D. Davis. Analysis of High Bay Hangar Facilities for Fire Detector Sensitivity and Placement. NIST Technical Note 1423, National Institute of Standards and Technology, Gaithersburg, Maryland, February 1997. [2](#), [91](#), [92](#)
- [21] R. Vettori. Effect of an Obstructed Ceiling on the Activation Time of a Residential Sprinkler. NISTIR 6253, National Institute of Standards and Technology, Gaithersburg, Maryland, November 1998. [2](#), [52](#), [93](#), [94](#)
- [22] S. Hostikka, M. Kokkala, and J. Vaari. Experimental Study of the Localized Room Fires. VTT Research Notes 2104, VTT Technical Research Centre of Finland, Espoo, Finland, 2001. [2](#), [24](#), [27](#), [95](#)
- [23] A. Hamins, A. Maranghides, K.B. McGrattan, E. Johnsson, T. Ohlemiller, M. Donnelly, J. Yang, G. Mulholland, K. Prasad, S. Kukuck, R. Anleitner, and T. McAllister. Federal Building and Fire Safety Investigation of the World Trade Center Disaster: Experiments and Modeling of Structural Steel Elements Exposed to Fire. NIST NCSTAR 1-5B, National Institute of Standards and Technology, Gaithersburg, Maryland, September 2005. [2](#), [36](#), [96](#), [97](#), [98](#), [99](#)

- [24] W.D. Walton and P.H. Thomas. *SFPE Handbook of Fire Protection Engineering*, chapter Estimating Temperatures in Compartment Fires. National Fire Protection Association, Quincy, Massachusetts, 4th edition, 2008. [3](#), [7](#), [10](#), [13](#), [70](#), [73](#), [76](#), [77](#), [82](#), [87](#), [96](#)
- [25] K. McGrattan and B. Toman. Quantifying the predictive uncertainty of complex numerical models. *Metrologia*, 48:173–180, 2011. [6](#)
- [26] W.D. Walton. ASET-B: A Room Fire Program for Personal Computers. NBSIR 85-3144, National Bureau of Standards (now NIST), Gaithersburg, Maryland, 1985. [17](#), [77](#)
- [27] J.A. Milke. *SFPE Handbook of Fire Protection Engineering*, chapter Smoke Management by Mechanical Exhaust or Natural Venting. National Fire Protection Association, Quincy, Massachusetts, 4th edition, 2008. [17](#)
- [28] F.W. Mowrer. *SFPE Handbook of Fire Protection Engineering*, chapter Enclosure Smoke Filling and Fire-Generated Environmental Conditions. National Fire Protection Association, Quincy, Massachusetts, 4th edition, 2008. [17](#)
- [29] E.E. Zukoski, T. Kubota, and B.M. Cetegen. Entrainment in fire plumes. *Fire Safety Journal*, 3(3):107–121, 1981. [17](#)
- [30] T. Tanaka and T. Yamana. Smoke Control in Large Scale Spaces (Part 1, Analytic theories for simple smoke control problems). *Fire Science and Technology*, 5(1):31–40, 1985. [20](#), [77](#)
- [31] G. Heskestad. *SFPE Handbook of Fire Protection Engineering*, chapter Fire Plumes, Flame Height and Air Entrainment. National Fire Protection Association, Quincy, Massachusetts, 4th edition, 2008. [23](#), [71](#), [85](#), [91](#), [92](#), [95](#)
- [32] B.J. McCaffrey. Purely Buoyant Diffusion Flames: Some Experimental Results. NBSIR 79-1910, National Bureau of Standards (now NIST), Gaithersburg, Maryland, October 1979. [26](#), [71](#), [85](#), [91](#), [92](#), [95](#)
- [33] J.A. Milke. *SFPE Handbook of Fire Protection Engineering*, chapter Analytical Methods for Determining Fire Resistance of Steel Members. National Fire Protection Association, Quincy, Massachusetts, 4th edition, 2008. [33](#), [35](#), [83](#), [86](#), [97](#), [98](#)
- [34] C.L. Beyler. *SFPE Handbook of Fire Protection Engineering*, chapter Fire Hazard Calculations for Large Open Hydrocarbon Fires. National Fire Protection Association, Quincy, Massachusetts, 4th edition, 2008. [39](#), [42](#), [69](#), [78](#), [99](#)
- [35] R.L. Alpert. *SFPE Handbook of Fire Protection Engineering*, chapter Ceiling Jet Flows. National Fire Protection Association, Quincy, Massachusetts, 4th edition, 2008. [47](#), [51](#), [65](#), [72](#), [79](#), [80](#), [81](#), [84](#), [89](#), [90](#), [93](#), [94](#), [100](#)
- [36] *Fire Protection Handbook*. National Fire Protection Association, Quincy, Massachusetts, 18th edition, 1997. [51](#)
- [37] R.W. Bukowski and J.D. Averill. Methods for Predicting Smoke Detector Activation. In *Proceedings of the Fire Suppression and Detection Research Application Symposium, Orlando, Florida*. National Fire Protection Association, Quincy, Massachusetts, 1998. [55](#), [81](#)

Appendix A

Validation Input Parameters

This appendix lists all of the input parameters that were used for each test in each data set. The input parameters are arranged alphabetically by data set, then by experimental quantity.

A.1 ATF Corridors

Ceiling Jet Temperature (Alpert) [35]

Table A.1: Summary of validation input parameters used for ATF Corridors cases [6], ceiling jet temperature.

Input Parameter	Value
Location Factor	1
r (m)	2, 9, 14.5
H (m)	2.03
T_{∞} (°C)	20

Test	\dot{Q} (kW)
ATF Corridors 50 kW	48
ATF Corridors 100 kW	97
ATF Corridors 240 kW	242
ATF Corridors 250 kW	250
ATF Corridors 500 kW	485

A.2 CAROLFIRE

Cable Failure Time [7]

The cable and conduit targets were not completely surrounded by the Penlight apparatus, which had openings at its ends. Therefore, the exposing temperature ramp T_{ramp} was calculated using a view factor of 0.90 and the experimentally measured shroud temperature.

Table A.2: Summary of validation input parameters used for CAROLFIRE cases [7], cable failure time.

Test	Cable Diameter (mm)	Mass per Unit Length (kg/m)	Jacket Thickness (mm)	Conduit Diameter (mm)	Conduit Thickness (mm)	T_{∞} (°C)	t_{end} (s)
Penlight Test 1	16.3	0.529	1.5	-	-	24	1800
Penlight Test 2	16.3	0.529	1.5	-	-	24	1800
Penlight Test 3	16.3	0.529	1.5	-	-	24	1800
Penlight Test 4	15.2	0.459	1.5	-	-	20	1800
Penlight Test 5	15.2	0.459	1.5	-	-	20	1800
Penlight Test 6	15.2	0.459	1.5	-	-	20	1800
Penlight Test 7	16.3	0.529	1.5	50	4.9	24	1800
Penlight Test 8	15.2	0.459	1.5	50	4.9	30	1800
Penlight Test 9	16.3	0.529	1.5	-	-	24	1800
Penlight Test 10	15.2	0.459	1.5	-	-	20	1800
Penlight Test 11	15.0	0.410	1.5	-	-	24	1800
Penlight Test 12	15.0	0.410	1.5	-	-	24	1800
Penlight Test 13	15.0	0.410	1.5	-	-	24	1800
Penlight Test 14	15.0	0.380	1.1	-	-	24	1800
Penlight Test 15	15.0	0.380	1.1	-	-	24	1800
Penlight Test 16	15.0	0.380	1.1	-	-	24	1800
Penlight Test 17	15.1	0.400	1.5	-	-	24	1800
Penlight Test 18	14.5	0.358	1.0	-	-	24	1800
Penlight Test 19	12.2	0.321	0.9	-	-	24	1800
Penlight Test 20	15.1	0.388	1.5	-	-	24	1800
Penlight Test 21	12.4	0.324	1.1	-	-	24	1190
Penlight Test 22	10.2	0.292	0.5	-	-	24	1640
Penlight Test 23	15.0	0.410	1.5	50	4.9	24	1800
Penlight Test 24	15.0	0.410	1.5	50	4.9	24	1800
Penlight Test 25	15.0	0.380	1.1	50	4.9	24	1800
Penlight Test 26	15.0	0.380	1.1	50	4.9	24	1800
Penlight Test 27	15.0	0.410	1.5	-	-	24	1800
Penlight Test 28	15.0	0.410	1.5	-	-	24	1800
Penlight Test 29	15.0	0.380	1.1	-	-	24	1640
Penlight Test 30	15.0	0.380	1.1	-	-	24	1800
Penlight Test 31	19.0	0.500	2.0	-	-	24	1800
Penlight Test 62	12.7	0.231	1.1	-	-	24	1190
Penlight Test 63	11.3	0.195	1.1	-	-	24	710
Penlight Test 64	7.9	0.097	1.1	-	-	24	890
Penlight Test 65	7.0	0.076	1.0	-	-	24	770

Table A.3: Summary of validation input parameters used for CAROLFIRE cases [7], cable failure time (continued).

Test	t_{ramp} (s)	T_{ramp} (°C)
Penlight Test 1	0, 70, 820, 1240, 1600, 1800	24, 460, 460, 275, 178, 0
Penlight Test 2	0, 80, 800, 1220, 1600, 1800	24, 460, 460, 275, 178, 0
Penlight Test 3	0, 80, 700, 950, 1600, 1800	24, 460, 460, 334, 178, 0
Penlight Test 4	0, 60, 820, 1470, 1800, 1900	24, 290, 290, 290, 188, 0
Penlight Test 5	0, 60, 820, 1080, 1600, 1800	24, 290, 290, 290, 139, 0
Penlight Test 6	0, 60, 820, 1080, 1600, 1800	24, 290, 290, 290, 139, 0
Penlight Test 7	0, 80, 820, 1240, 1800, 1900	24, 460, 460, 460, 460, 0
Penlight Test 8	0, 55, 820, 1080, 1800, 1900	24, 290, 290, 290, 290, 0
Penlight Test 9	0, 80, 820, 1240, 1800, 1900	24, 451, 451, 451, 451, 0
Penlight Test 10	0, 60, 820, 1500, 1800, 1900	24, 285, 285, 285, 188, 0
Penlight Test 11	0, 80, 820, 1320, 1800, 1900	24, 456, 456, 456, 266, 0
Penlight Test 12	0, 80, 820, 1320, 1800, 1900	24, 460, 460, 460, 266, 0
Penlight Test 13	0, 80, 820, 1320, 1800, 1900	24, 460, 460, 460, 266, 0
Penlight Test 14	0, 60, 820, 1470, 1800, 1900	24, 290, 290, 290, 290, 0
Penlight Test 15	0, 60, 820, 1470, 1800, 1900	24, 314, 314, 314, 188, 0
Penlight Test 16	0, 60, 820, 1470, 1800, 1900	24, 314, 314, 314, 314, 0
Penlight Test 17	0, 80, 660, 1240, 1600, 1800	24, 460, 460, 275, 178, 0
Penlight Test 18	0, 70, 820, 1240, 1600, 1800	24, 675, 675, 675, 675, 0
Penlight Test 19	0, 80, 820, 1050, 1500, 1800	24, 460, 460, 460, 236, 0
Penlight Test 20	0, 70, 600, 1240, 1600, 1800	24, 460, 460, 275, 178, 0
Penlight Test 21	0, 60, 930, 1200	24, 290, 290, 197
Penlight Test 22	0, 80, 1440, 1650	24, 460, 460, 295
Penlight Test 23	0, 80, 1801	24, 456, 456
Penlight Test 24	0, 80, 1801	24, 456, 456
Penlight Test 25	0, 50, 1801	24, 309, 309
Penlight Test 26	0, 60, 1801	24, 309, 309
Penlight Test 27	0, 80, 1500, 1801	24, 456, 456, 305
Penlight Test 28	0, 80, 1801	24, 451, 451
Penlight Test 29	0, 60, 1260, 1650	24, 309, 309, 188
Penlight Test 30	0, 50, 1350, 1800	24, 309, 309, 188
Penlight Test 31	0, 70, 820, 1240, 1600, 1801	24, 675, 675, 675, 675, 0
Penlight Test 62	0, 80, 300, 480, 1200	24, 451, 451, 334, 207
Penlight Test 63	0, 70, 720	24, 309, 309
Penlight Test 64	0, 80, 240, 900	24, 451, 451, 207
Penlight Test 65	0, 65, 540, 780	24, 309, 309, 217

A.3 Fleury Heat Flux

Point Source and Solid Flame Radiation Heat Flux [34]

Table A.4: Summary of validation input parameters used for Fleury Heat Flux cases [8], radiation heat flux.

Input Parameter	Value
χ_r	0.35
x (m)	0.5, 0.75, 1.0, 1.5, 2.0
z (m)	0.0, 0.5, 1.0, 1.5
IOR	2

Test	\dot{Q} (kW)	A (m ²)
100 kW, 1:1 Burner	100	0.09
150 kW, 1:1 Burner	150	0.09
200 kW, 1:1 Burner	200	0.09
250 kW, 1:1 Burner	250	0.09
300 kW, 1:1 Burner	300	0.09
100 kW, 2:1 Burner	100	0.18
150 kW, 2:1 Burner	150	0.18
200 kW, 2:1 Burner	200	0.18
250 kW, 2:1 Burner	250	0.18
300 kW, 2:1 Burner	300	0.18
100 kW, 3:1 Burner	100	0.27
150 kW, 3:1 Burner	150	0.27
200 kW, 3:1 Burner	200	0.27
250 kW, 3:1 Burner	250	0.27
300 kW, 3:1 Burner	300	0.27

A.4 FM/SNL

HGL Temperature [24]

Table A.5: Summary of validation input parameters used for FM/SNL cases [9, 10], HGL temperature.

Input Parameter	Value
L (m)	18.3
W (m)	12.2
H (m)	6.1
c_p (kJ/(kg · K))	1.0
k (kW/(m · K))	0.00023
ρ (kg/m ³)	1000
c (kJ/(kg · K))	1.16
δ (m)	0.025

Test	Correlation	\dot{Q} (kW)	\dot{m} (kg/s)	T_∞ (°C)	t_{end} (s)
Test 1	FPA, DB	516	4.5	15	600
Test 2	FPA, DB	516	4.5	14	600
Test 3	FPA, DB	2000	4.5	15	300
Test 4	FPA, DB	516	0.45	15	600
Test 5	FPA, DB	516	4.5	19	600
Test 6	FPA, DB	500	0.45	15	600
Test 7	FPA, DB	516	0.45	15	600
Test 8	FPA, DB	1000	0.45	21	720
Test 9	FPA, DB	1000	3.6	24	840
Test 10	FPA, DB	1000	2.0	18	600
Test 11	FPA, DB	500	2.0	16	600
Test 12	FPA, DB	2000	2.0	17	600
Test 13	FPA, DB	2000	3.6	21	600
Test 14	FPA, DB	500	0.45	15	600
Test 15	FPA, DB	1000	0.45	18	1380
Test 16	FPA, DB	500	0.45	18	720
Test 17	FPA, DB	500	4.5	10	1380
Test 21	FPA, DB	500	0.45	14	1200
Test 22	FPA, DB	1000	0.45	14	840

Plume Temperature (Heskestad and McCaffrey) [31, 32]

Table A.6: Summary of validation input parameters used for FM/SNL cases [9, 10], plume temperature.

Input Parameter	Value
z (m)	5.98
A (m ²)	0.64
χ_r	0.35
c_p (kJ/(kg · K))	1.0

Test	\dot{Q} (kW)	T_∞ (°C)
Test 1	516	15
Test 2	516	14
Test 3	2000	15
Test 4	516	15
Test 5	516	19
Test 6	500	15
Test 7	516	15
Test 8	1000	21
Test 9	1000	24
Test 10	1000	18
Test 11	500	16
Test 12	2000	17
Test 13	2000	21
Test 14	500	15
Test 15	1000	18
Test 16	500	18
Test 17	500	10
Test 21	500	14
Test 22	1000	14

Ceiling Jet Temperature (Alpert) [35]

Table A.7: Summary of validation input parameters used for FM/SNL cases [9, 10], ceiling jet temperature.

Input Parameter	Value
r (m)	3.05, 9.15
H (m)	5.9

Test	\dot{Q} (kW)	Location Factor	T_{∞} (°C)
Test 1	516	1	15
Test 2	516	1	14
Test 3	2000	1	15
Test 4	516	1	15
Test 5	516	1	19
Test 6	500	2	15
Test 7	516	1	15
Test 8	1000	1	21
Test 9	1000	1	24
Test 10	1000	2	18
Test 11	500	2	16
Test 12	2000	2	17
Test 13	2000	2	21
Test 14	500	2	15
Test 15	1000	2	18
Test 16	500	4	18
Test 17	500	4	10
Test 21	500	1	14
Test 22	1000	1	14

A.5 LLNL Enclosure

HGL Temperature [24]

For the cases with natural ventilation (MQH), the door size was 2.06 m high by 0.76 m wide.

Table A.8: Summary of validation input parameters used for LLNL Enclosure cases [11], HGL temperature.

Input Parameter	Value
c_p (kJ/(kg · K))	1.0
k (kW/(m · K))	0.000463
ρ (kg/m ³)	1607
c (kJ/(kg · K))	1.0
δ (m)	0.1
Location Factor	1
Heat Loss Fraction	0
Fuel Height	0

Test	Correlation	\dot{Q} (kW)	L (m)	W (m)	H (m)	\dot{m} (kg/s)	T_∞ (°C)	t_{end} (s)
Test 1	Beyler	200	6.0	4.0	4.5	-	23	500
Test 2	Beyler	200	6.0	4.0	4.5	-	27	500
Test 3	Beyler	400	6.0	4.0	4.5	-	27	200
Test 4	Beyler	300	6.0	4.0	4.5	-	24	300
Test 5	Beyler	50	6.0	4.0	4.5	-	28	2500
Test 6	Beyler	100	6.0	4.0	4.5	-	29	1000
Test 7	Beyler	100	6.0	4.0	4.5	-	35	1000
Test 8	Beyler	200	6.0	4.0	4.5	-	35	500
Test 9	FPA, DB	200	6.0	4.0	4.5	0.565	33	4000
Test 10	FPA, DB	200	6.0	4.0	4.5	0.118	28	6000
Test 11	FPA, DB	200	6.0	4.0	4.5	0.240	18	4000
Test 12	FPA, DB	200	6.0	4.0	4.5	0.366	21	5000
Test 13	FPA, DB	200	6.0	4.0	4.5	0.474	28	5000
Test 14	FPA, DB	200	6.0	4.0	4.5	0.472	28	5000
Test 15	FPA, DB	100	6.0	4.0	4.5	0.352	24	4000
Test 16	FPA, DB	200	6.0	4.0	4.5	0.356	21	6000
Test 17	FPA, DB	200	6.0	4.0	3.0	0.587	26	3000
Test 18	FPA, DB	200	6.0	4.0	3.0	0.463	21	4000
Test 19	FPA, DB	200	6.0	4.0	3.0	0.351	18	5000
Test 20	FPA, DB	200	6.0	4.0	3.0	0.240	16	6000
Test 21	FPA, DB	200	6.0	4.0	3.0	0.116	23	6000
Test 22	FPA, DB	200	6.0	4.0	3.0	0.225	30	500
Test 23	FPA, DB	200	6.0	4.0	3.0	0.249	28	4000
Test 24	FPA, DB	200	6.0	4.0	3.0	0.235	26	1000
Test 25	FPA, DB	200	6.0	4.0	3.0	0.233	25	2000

Test	Correlation	\dot{Q} (kW)	L (m)	W (m)	H (m)	\dot{m} (kg/s)	T_{∞} (°C)	t_{end} (s)
Test 26	FPA, DB	200	6.0	4.0	3.0	0.586	24	4000
Test 27	FPA, DB	200	6.0	4.0	3.0	0.116	23	500
Test 28	FPA, DB	150	6.0	4.0	3.0	0.174	31	1000
Test 29	FPA, DB	250	6.0	4.0	3.0	0.298	28	1000
Test 30	FPA, DB	250	6.0	4.0	3.0	0.349	34	4000
Test 31	FPA, DB	250	6.0	4.0	3.0	0.576	36	4000
Test 32	FPA, DB	100	6.0	4.0	3.0	0.110	33	4000
Test 33	FPA, DB	100	6.0	4.0	3.0	0.230	23	5000
Test 34	FPA, DB	100	6.0	4.0	3.0	0.342	34	4000
Test 35	FPA, DB	100	6.0	4.0	3.0	0.455	22	4000
Test 36	FPA, DB	100	6.0	4.0	3.0	0.582	29	4000
Test 37	FPA, DB	170	6.0	4.0	3.0	0.111	20	500
Test 38	FPA, DB	200	6.0	4.0	3.0	0.346	29	4000
Test 39	FPA, DB	250	6.0	4.0	3.0	0.107	18	500
Test 40	FPA, DB	200	6.0	4.0	3.0	0.467	28	4000
Test 41	FPA, DB	150	6.0	4.0	3.0	0.126	20	500
Test 42	FPA, DB	200	6.0	4.0	3.0	0.206	30	5000
Test 43	Beyler	200	6.0	4.0	3.0	-	32	500
Test 44	FPA, DB	200	6.0	4.0	3.0	0.213	19	2000
Test 45	Beyler	200	6.0	4.0	3.0	-	30	500
Test 46	FPA, DB	200	6.0	4.0	3.0	0.201	19	500
Test 47	Beyler	200	6.0	4.0	3.0	-	19	500
Test 48	Beyler	165	6.0	4.0	3.0	-	21	500
Test 49	FPA, DB	200	6.0	4.0	3.0	0.208	26	500
Test 50	FPA, DB	200	6.0	4.0	3.0	0.222	21	4000
Test 51	MQH	200	6.0	4.0	3.0	-	33	3000
Test 52	MQH	200	6.0	4.0	3.0	-	23	4000
Test 53	FPA, DB	200	6.0	4.0	3.0	0.214	33	1000
Test 54	FPA, DB	200	6.0	4.0	3.0	0.248	21	4000
Test 55	MQH	100	6.0	4.0	3.0	-	31	4000
Test 56	FPA, DB	200	6.0	4.0	3.0	0.221	20	1000
Test 57	FPA, DB	200	6.0	4.0	3.0	0.247	29	5000
Test 58	FPA, DB	200	6.0	4.0	3.0	0.220	18	4000
Test 59	FPA, DB	200	6.0	4.0	3.0	0.214	24	4000
Test 60	MQH	400	6.0	4.0	3.0	-	22	2000
Test 61	MQH	200	6.0	4.0	4.5	-	31	2000
Test 62	MQH	400	6.0	4.0	4.5	-	22	2000
Test 63	MQH	50	6.0	4.0	4.5	-	28	3000
Test 64	MQH	100	6.0	4.0	4.5	-	17	3000

A.6 NBS Multi-Room

HGL Temperature [24]

Table A.9: Summary of validation input parameters used for NBS Multi-Room cases [12], HGL temperature.

Input Parameter	Value
\dot{Q} (kW)	100
L (m)	2.34
W (m)	2.34
H (m)	2.16
H_o (m)	1.6
W_o (m)	0.81
k (kW/(m · K))	0.00017
ρ (kg/m ³)	128
c (kJ/(kg · K))	1.04
δ (m)	0.05
t_{end} (s)	1200

Test	Correlation	T_{∞} (°C)
Test 100A	MQH	23
Test 100O	MQH	21
Test 100Z	MQH	22

A.7 NIST/NRC

HGL Temperature and Depth [24, 26, 30]

For the cases with natural ventilation (MQH), the door size was 2.0 m high by 2.0 m wide.

Table A.10: Summary of validation input parameters used for NIST/NRC cases [13], HGL temperature and depth.

Input Parameter	Value
L (m)	21.66
W (m)	7.04
H (m)	3.82
c_p (kJ/(kg · K))	1.0
k (kW/(m · K))	0.00012
ρ (kg/m ³)	737
c (kJ/(kg · K))	1.42
δ (m)	0.0254
Location Factor	1
Heat Loss Fraction	0
Fuel Height	0

Test	Correlation	\dot{Q} (kW)	\dot{m} (kg/s)	H_o (m)	W_o (m)	T_∞ (°C)	t_{end} (s)
Test 1	Beyler	410	-	-	-	22	1350
Test 2	Beyler	1190	-	-	-	26	625
Test 3	MQH	1190	-	2.0	2.0	30	1380
Test 4	FPA, DB	1200	1.3	-	-	27	816
Test 5	MQH	1190	-	2.0	2.0	28	1380
Test 7	Beyler	400	-	-	-	24	1330
Test 8	Beyler	1190	-	-	-	25	610
Test 9	MQH	1170	-	2.0	2.0	27	1380
Test 10	FPA, DB	1190	1.3	-	-	27	826
Test 13	Beyler	2330	-	-	-	31	265
Test 14	MQH	1180	-	2.0	2.0	28	1380
Test 15	MQH	1180	-	2.0	2.0	18	1380
Test 16	FPA, DB	2300	1.3	-	-	26	380
Test 17	Beyler	1160	-	-	-	29	272
Test 18	MQH	1180	-	2.0	2.0	27	1380

Point Source and Solid Flame Radiation Heat Flux [34]

Table A.11: Summary of validation input parameters used for NIST/NRC cases [13], radiation heat flux.

Input Parameter	Value
x (m)	3.14, 2.33, 2.18, 1.58, 3.27
z (m)	2.05, 2.52, 2.54, 3.04, 1.76
IOR	-3, -3, 2, -3, -2

Test	\dot{Q} (kW)	χ_r	A (m ²)
Test 1	410	0.44	0.671
Test 2	1190	0.44	1.028
Test 3	1190	0.44	1.028
Test 4	1200	0.44	1.032
Test 5	1190	0.44	1.028
Test 7	400	0.44	0.665
Test 8	1190	0.44	1.028
Test 9	1170	0.44	1.021
Test 10	1190	0.44	1.028
Test 13	2330	0.44	1.345
Test 14	1180	0.44	1.025
Test 15	1180	0.44	1.025
Test 16	2300	0.44	1.338
Test 17	1160	0.40	1.018
Test 18	1180	0.44	1.025

Ceiling Jet Temperature (Alpert) [35]

Table A.12: Summary of validation input parameters used for NIST/NRC cases [13], ceiling jet temperature.

Input Parameter	Value
Location Factor	1
r (m)	5.9
H (m)	3.72

Test	\dot{Q} (kW)	T_{∞} (°C)
Test 1	410	22
Test 2	1190	26
Test 3	1190	30
Test 4	1200	27
Test 5	1190	28
Test 7	400	24
Test 8	1190	25
Test 9	1170	27
Test 10	1190	27
Test 13	2330	31
Test 14	1180	28
Test 15	1180	18
Test 16	2300	26
Test 17	1160	29
Test 18	1180	27

A.8 NIST Smoke Alarms

Ceiling Jet Temperature (Alpert) [35]

Table A.13: Summary of validation input parameters used for NIST Smoke Alarms cases [14], ceiling jet temperature.

Input Parameter	Value
Location Factor	1
H (m)	2.1
t_{end} (s)	300

Test	α (kW/s ²)	r (m)	T_{∞} (°C)
Test SDC02	0.00463	1.15	21
Test SDC05	0.00617	1.25	22
Test SDC07	0.01080	1.25	24
Test SDC10	0.00463	1.15	26
Test SDC33	0.00309	1.15	26
Test SDC35	0.00309	1.15	26
Test SDC38	0.00370	1.25	25
Test SDC39	0.00617	1.25	25

Smoke Detector Activation Time (Temperature Rise) [35, 37]

The fire growth was specified as $\dot{Q} = \alpha t^2$ up to a cutoff time of t_{fire} . After the time t_{fire} , the fire HRR was steady.

Table A.14: Summary of validation input parameters used for NIST Smoke Alarms cases [14], smoke detector activation time.

Input Parameter	Value
Location Factor	1
t_{fire} (s)	300
ΔT_c ($^{\circ}\text{C}$)	5
RTI ($(\text{m} \cdot \text{s})^{1/2}$)	5

Test	α (kW/s^2)	r (m)	H (m)	T_{∞} ($^{\circ}\text{C}$)
Test SDC02	0.00463	1.3	2.1	21
Test SDC05	0.00617	1.8	2.0	22
Test SDC07	0.01080	1.8	2.0	24
Test SDC10	0.00463	1.3	2.1	26
Test SDC33	0.00309	1.3	2.1	26
Test SDC35	0.00309	1.3	2.1	26
Test SDC38	0.00370	1.3	2.1	25
Test SDC39	0.00617	1.8	2.0	25

A.9 SP AST

HGL Temperature [24]

Table A.15: Summary of validation input parameters used for SP AST cases, HGL temperature.

Input Parameter	Value
\dot{Q} (kW)	450
L (m)	3.6
W (m)	3.6
H (m)	2.4
H_o (m)	2.0
W_o (m)	0.8
k (kW/(m · K))	0.0001
ρ (kg/m ³)	600
c (kJ/(kg · K))	0.8
δ (m)	0.2
T_∞ (°C)	20

Test	Correlation	t_{end} (s)
Test 1	MQH	2400
Test 2	MQH	2400
Test 3	MQH	3600

Steel Temperature (Unprotected) [33]

The HGL temperatures from the MQH HGL temperature correlation were used as the input fire temperature T_f .

Table A.16: Summary of validation input parameters used for SP AST cases [15], unprotected steel temperature.

Input Parameter	Value
ρ_s (kg/m ³)	7833
c_s (kJ/(kg · K))	0.465
ϵ	0.7
h_c (W/(m ² · K))	25

Test	Correlation for T_f	F/V (1/m)	t_{end} (s)
Test 1	MQH	125	2400
Test 2	MQH	157	2400
Test 3	MQH	157	3600

Ceiling Jet Temperature (Alpert) [35]

Table A.17: Summary of validation input parameters used for SP AST cases [15], ceiling jet temperature.

Input Parameter	Value
\dot{Q} (kW)	450
H (m)	1.65
T_{∞} ($^{\circ}\text{C}$)	20

Test	Location Factor	r (m)
Test 1	4	1.22
Test 2	4	1.22
Test 3	2	0.70

A.10 SP AST Column

Plume Temperature (Heskestad and McCaffrey) [31, 32]

Note that the Heskestad correlation did not use heights of 1 m and 2 m because it is valid only above the flame region.

Table A.18: Summary of validation input parameters used for SP AST Column cases [16], plume temperature.

Input Parameter	Value
z (m)	1, 2, 3, 4, 5
χ_r	0.35
c_p (kJ/(kg · K))	1.0
T_∞ (°C)	20

Test	\dot{Q} (kW)	A (m ²)
Diesel, 1.1 m	1434	0.95
Diesel, 1.9 m	1873	0.95
Heptane, 1.1 m	2275	2.83

Steel Temperature (Unprotected) [33]

The HGL temperatures from the McCaffrey plume temperature correlation were used as the input fire temperature T_f .

Table A.19: Summary of validation input parameters used for SP AST Column cases [16], unprotected steel temperature.

Input Parameter	Value
F/V (1/m)	205
ρ_s (kg/m ³)	7833
c_s (kJ/(kg · K))	0.465
ϵ	0.7
h_c (W/(m ² · K))	25

Test	Correlation for T_f	\dot{Q} (kW)	t_{end} (s)
Diesel, 1.1 m	McCaffrey	1434	1620
Diesel, 1.9 m	McCaffrey	1873	1080
Heptane, 1.1 m	McCaffrey	2275	900

A.11 Steckler

HGL Temperature [24]

Table A.20: Summary of validation input parameters used for Steckler cases [17], HGL temperature.

Input Parameter	Value
L (m)	2.8
W (m)	2.8
H (m)	2.13
k (kW/(m · K))	0.0001
ρ (kg/m ³)	200
c (kJ/(kg · K))	1.0
δ (m)	0.013

Test	Correlation	\dot{Q} (kW)	H_o (m)	W_o (m)	T_∞ (°C)
Test 10	MQH	62.9	1.83	0.24	22
Test 11	MQH	62.9	1.83	0.36	25
Test 12	MQH	62.9	1.83	0.49	19
Test 612	MQH	62.9	1.83	0.49	19
Test 13	MQH	62.9	1.83	0.62	20
Test 14	MQH	62.9	1.83	0.74	28
Test 18	MQH	62.9	1.83	0.74	29
Test 710	MQH	62.9	1.83	0.74	13
Test 810	MQH	62.9	1.83	0.74	15
Test 16	MQH	62.9	1.83	0.86	23
Test 17	MQH	62.9	1.83	0.99	19
Test 22	MQH	62.9	1.38	0.74	26
Test 23	MQH	62.9	0.92	0.74	23
Test 30	MQH	62.9	0.92	0.74	23
Test 41	MQH	62.9	0.46	0.74	14
Test 19	MQH	31.6	1.83	0.74	29
Test 20	MQH	105.3	1.83	0.74	29
Test 21	MQH	158.	1.83	0.74	29
Test 114	MQH	62.9	1.83	0.24	31
Test 144	MQH	62.9	1.83	0.36	30
Test 212	MQH	62.9	1.83	0.49	25
Test 242	MQH	62.9	1.83	0.62	29
Test 410	MQH	62.9	1.83	0.74	21

Test	Correlation	\dot{Q} (kW)	H_o (m)	W_o (m)	T_∞ (°C)
Test 210	MQH	62.9	1.83	0.74	30
Test 310	MQH	62.9	1.83	0.74	20
Test 240	MQH	62.9	1.83	0.86	28
Test 116	MQH	62.9	1.83	0.99	29
Test 122	MQH	62.9	1.38	0.74	27
Test 224	MQH	62.9	0.92	0.74	26
Test 324	MQH	62.9	0.92	0.74	22
Test 220	MQH	31.6	1.83	0.74	25
Test 221	MQH	105.3	1.83	0.74	25
Test 514	MQH	62.9	1.83	0.24	8
Test 544	MQH	62.9	1.83	0.36	8
Test 512	MQH	62.9	1.83	0.49	20
Test 542	MQH	62.9	1.83	0.62	20
Test 610	MQH	62.9	1.83	0.74	18
Test 510	MQH	62.9	1.83	0.74	22
Test 540	MQH	62.9	1.83	0.86	13
Test 517	MQH	62.9	1.83	0.99	14
Test 622	MQH	62.9	1.38	0.74	9
Test 522	MQH	62.9	1.38	0.74	13
Test 524	MQH	62.9	0.92	0.74	8
Test 541	MQH	62.9	0.46	0.74	7
Test 520	MQH	31.6	1.83	0.74	17
Test 521	MQH	105.3	1.83	0.74	13
Test 513	MQH	158.	1.83	0.74	14
Test 160	MQH	62.9	1.83	0.74	6
Test 163	MQH	62.9	1.83	0.74	6
Test 164	MQH	62.9	1.83	0.74	6
Test 165	MQH	62.9	1.83	0.74	6
Test 162	MQH	62.9	1.83	0.74	6
Test 167	MQH	62.9	1.83	0.74	6
Test 161	MQH	62.9	1.83	0.74	6
Test 166	MQH	62.9	1.83	0.74	6

A.12 UL/NFPRF

Ceiling Jet Temperature (Alpert) [35]

Table A.21: Summary of validation input parameters used for UL/NFPRF cases [18, 19], ceiling jet temperature.

Input Parameter	Value
Location Factor	1
r (m)	2.12, 4.74, 6.36, 10.61, 12.90, 13.58, 14.23, 14.85, 17.10, 19.09, 21.32
H (m)	7.1
T_{∞} (°C)	18

Test	\dot{Q} (kW)
I-17	4600
I-18	3700
I-19	4600
I-20	4200
I-21	4600
I-22	4600

Sprinkler Activation Time [35]

The fire growth was specified as $\dot{Q} = \alpha t^2$ up to a cutoff time of t_{fire} . After the time t_{fire} , the fire HRR was steady.

Table A.22: Summary of validation input parameters used for UL/NFPRF cases [18, 19], sprinkler activation time.

Input Parameter	Value
α (kW/s ²)	1.778
Location Factor	1
RTI ((m · s) ^{1/2})	148
T_{act} (°C)	74
H (m)	7.0
T_{∞} (°C)	18

Test	t_{fire} (s)	r (m)	Test	t_{fire} (s)	r (m)
I-1	50	2.12	II-1	75	1.5
I-2	50	2.12	II-2	75	1.5
I-3	50	2.12	II-3	75	1.5
I-4	50	2.12	II-4	75	1.5
I-5	50	2.12	II-5	75	1.5
I-6	50	2.12	II-6	75	1.5
I-7	50	2.12	II-7	75	1.5
I-8	50	2.12	II-8	75	1.5
I-9	50	2.12	II-9	75	2.12
I-10	50	2.12	II-10	75	2.12
I-11	50	2.12	II-11	75	1.5
I-12	50	2.12	II-12	75	1.5
I-13	58	2.12			1.5
I-14	57	2.12			1.5
I-15	57	2.12			1.5
I-16	106	2.12			1.5
I-17	51	2.12			1.5
I-18	47	2.12			1.5
I-19	51	2.12			1.5
I-20	49	2.12			1.5
I-21	51	2.12			1.5
I-22	51	2.12			1.5

A.13 USN Hawaii

Plume Temperature (Heskestad and McCaffrey) [31, 32]

The fire growth was specified as $\dot{Q} = \alpha t^2$ up to a cutoff time of t_{fire} . After the time t_{fire} , the fire HRR was steady.

Table A.23: Summary of validation input parameters used for USN Hawaii cases [20], plume temperature.

Input Parameter	Value
z (m)	8.7, 11.8, 13.3, 14.5
χ_r	0.35
c_p (kJ/(kg · K))	1.0

Test	α (kW/s ²)	t_{fire} (s)	\dot{Q} (kW)	A (m ²)	T_{∞} (°C)
Test 1	0.00694	120	100	0.09	27
Test 2	0.02222	150	500	0.36	28
Test 3	0.04889	150	1100	0.81	27
Test 4	0.09133	180	2959	1.69	27
Test 5	0.48597	120	6998	3.24	27
Test 6	0.33773	150	7599	4.84	25
Test 7	0.17799	180	5767	3.24	30
Test 11	0.00444	150	100	0.09	30

A.14 USN Iceland

Plume Temperature (Heskestad and McCaffrey) [31, 32]

Table A.24: Summary of validation input parameters used for USN Hawaii cases [20], plume temperature.

Input Parameter	Value
z (m)	15.7, 17.2, 18.8, 20.3, 21.5
χ_r	0.35
c_p (kJ/(kg · K))	1.0

Test	\dot{Q} (kW)	A (m ²)	T_∞ (°C)
Test 1	88	0.09	10
Test 2	60	0.09	10
Test 3	720	0.36	11
Test 4	684	0.36	14
Test 5	1134	0.81	17
Test 6	1296	0.81	16
Test 7	2736	1.44	16
Test 9	153	0.09	9
Test 10	612	0.36	9
Test 11	648	0.36	9
Test 12	1512	0.36	9
Test 13	2700	1.44	11
Test 14	7802	4.84	12
Test 15	15300	9.00	12
Test 17	15750	9.00	11
Test 18	4918	3.24	10
Test 19	8712	4.84	13
Test 20	14850	9.00	14

A.15 Vettori Flat Ceiling

Ceiling Jet Temperature (Alpert) [35]

Table A.25: Summary of validation input parameters used for Vettori Flat cases [21], ceiling jet temperature.

Only the smooth, unobstructed ceiling tests were included in this study. The fire growth was specified as $\dot{Q} = \alpha t^2$ up to a cutoff time of t_{fire} . After the time t_{fire} , the fire HRR was steady.

Input Parameter	Value
H (m)	2.075

Test	α (kW/s ²)	t_{fire} (s)	r (m)	Location Factor	T_{∞} (°C)
Test 1	0.105	50	2.2, 2.2	1	16.6
Test 2	0.105	50	2.2, 2.2	1	19.0
Test 3	0.105	50	2.2, 2.2	1	20.8
Test 6	0.017	80	2.2, 2.2	1	17.1
Test 7	0.017	80	2.2, 2.2	1	21.6
Test 8	0.017	80	2.2, 2.2	1	21.8
Test 11	0.0041	100	2.2, 2.2	1	18.1
Test 12	0.0041	140	2.2, 2.2	1	21.0
Test 13	0.0041	130	2.2, 2.2	1	22.0
Test 16	0.105	45	2.4, 2.4	2	20.7
Test 17	0.105	42	2.4, 2.4	2	20.4
Test 18	0.105	35	2.4, 2.4	2	20.3
Test 21	0.017	70	2.4, 2.4	2	21.1
Test 22	0.017	70	2.4, 2.4	2	21.7
Test 23	0.017	70	2.4, 2.4	2	21.8
Test 26	0.0041	130	2.4, 2.4	2	21.5
Test 27	0.0041	130	2.4, 2.4	2	22.5
Test 28	0.0041	120	2.4, 2.4	2	22.7
Test 31	0.105	37	2.1, 6.59	4	20.2
Test 32	0.105	30	2.1, 6.59	4	21.9
Test 33	0.105	30	2.1, 6.59	4	21.7
Test 36	0.017	50	2.1, 6.59	4	22.3
Test 37	0.017	47	2.1, 6.59	4	22.3
Test 38	0.017	50	2.1, 6.59	4	21.7
Test 41	0.0041	100	2.1, 6.59	4	21.6
Test 42	0.0041	85	2.1, 6.59	4	22.4
Test 43	0.0041	85	2.1, 6.59	4	21.6

Sprinkler Activation Time [35]

The fire growth was specified as $\dot{Q} = \alpha t^2$ up to the time of the first sprinkler activation.

Table A.26: Summary of validation input parameters used for Vettori Flat cases [21], sprinkler activation time.

Input Parameter	Value
RTI ((m · s) ^{1/2})	55
T_{act} (°C)	68
H (m)	2.09

Test	α (kW/s ²)	r (m)	Location Factor	T_{∞} (°C)
Test 1	0.105	2.2	1	16.6
Test 2	0.105	2.2	1	19.0
Test 3	0.105	2.2	1	20.8
Test 6	0.017	2.2	1	17.1
Test 7	0.017	2.2	1	21.6
Test 8	0.017	2.2	1	21.8
Test 11	0.0041	2.2	1	18.1
Test 12	0.0041	2.2	1	21.0
Test 13	0.0041	2.2	1	22.0
Test 16	0.105	2.4	2	20.7
Test 17	0.105	2.4	2	20.4
Test 18	0.105	2.4	2	20.3
Test 21	0.017	2.4	2	21.1
Test 22	0.017	2.4	2	21.7
Test 23	0.017	2.4	2	21.8
Test 26	0.0041	2.4	2	21.5
Test 27	0.0041	2.4	2	22.5
Test 28	0.0041	2.4	2	22.7
Test 31	0.105	2.1	4	20.2
Test 32	0.105	2.1	4	21.9
Test 33	0.105	2.1	4	21.7
Test 36	0.017	2.1	4	22.3
Test 37	0.017	2.1	4	22.3
Test 38	0.017	2.1	4	21.7
Test 41	0.0041	2.1	4	21.6
Test 42	0.0041	2.1	4	22.4
Test 43	0.0041	2.1	4	21.6

A.16 VTT Large Hall

Plume Temperature (Heskestad and McCaffrey) [31, 32]

The fire ramp was specified as \dot{Q}_{ramp} with a corresponding t_{ramp} . For example, a fire growing linearly over time 0 s to 100 s from 0 kW to 500 kW would be specified with a t_{ramp} of [0, 100] and a \dot{Q}_{ramp} of [0, 500].

Table A.27: Summary of validation input parameters used for VTT Large Hall cases [22], plume temperature.

Input Parameter	Value
z (m)	6, 12
χ_r	0.40
c_p (kJ/(kg · K))	1.0

Test	t_{ramp} (s)	\dot{Q}_{ramp} (kW)	A (m ²)	T_{∞} (°C)
Test 1	13, 90, 288, 327, 409	1245, 1309, 1858, 1783, 1356	1.075	25
Test 2	14, 30, 91, 193, 282, 340, 372	2151, 2542, 3063, 3259, 3129, 2737, 2281	2.01	22
Test 3	13, 63, 166, 256, 292, 330	2437, 3201, 3601, 3638, 3456, 2656	2.01	22

A.17 WTC

HGL Temperature [24]

Table A.28: Summary of validation input parameters used for WTC cases [23], HGL temperature.

Input Parameter	Value
L (m)	7.04
W (m)	3.60
H (m)	3.82
H_o (m)	2.82
W_o (m)	2.4
k (kW/(m · K))	0.00012
ρ (kg/m ³)	737
c (kJ/(kg · K))	1.42
δ (m)	0.0254

Test	Correlation	\dot{Q} (kW)	t_{end} (s)	T_{∞} (°C)
Test 1	MQH	2000	870	24
Test 2	MQH	2400	380	25
Test 3	MQH	2000	990	20
Test 4	MQH	3200	840	20
Test 5	MQH	3000	3080	20
Test 6	MQH	3000	3030	20

Steel Temperature (Unprotected) [33]

The HGL temperatures from the MQH HGL temperature correlation were used as the input fire temperature T_f . The inputs for the MQH correlation are described in the WTC HGL temperature section.

Table A.29: Summary of validation input parameters used for WTC cases [23], unprotected steel temperature.

Input Parameter	Value
ρ_s (kg/m ³)	7860
c_s (kJ/(kg · K))	0.450
ε	0.7
h_c (W/(m ² · K))	25

Test	Correlation for T_f	Structural Element	F/V (1/m)
Test 1	MQH	Bar	157
Test 2	MQH	Bar	157
Test 3	MQH	Bar	157
Test 1	MQH	Column	159
Test 2	MQH	Column	159
Test 3	MQH	Column	159
Test 1	MQH	Truss A	156
Test 2	MQH	Truss A	156
Test 3	MQH	Truss A	156
Test 1	MQH	Truss B	156
Test 2	MQH	Truss B	156
Test 3	MQH	Truss B	156

Steel Temperature (Protected) [33]

The HGL temperatures from the MQH HGL temperature correlation were used as the input fire temperature T_f . The inputs for the MQH correlation are described in the WTC HGL temperature section.

Table A.30: Summary of validation input parameters used for WTC cases [23], protected steel temperature.

Input Parameter	Value
c_s (kJ/(kg · K))	0.450
k_i (W/(m · K))	0.10
ρ_i (kg/m ³)	208
c_i (kJ/(kg · K))	2.0

Test	Correlation for T_f	Structural Element	h_i (m)	W/D (kg/m ²)
Test 4	MQH	Bar	0.0191	50.1
Test 5	MQH	Bar	0.0191	50.1
Test 6	MQH	Bar	0.0191	50.1
Test 4	MQH	Column	0.0381	49.4
Test 5	MQH	Column	0.0381	49.4
Test 6	MQH	Column	0.0381	49.4
Test 4	MQH	Truss A	0.0191	50.3
Test 5	MQH	Truss A	0.0191	50.3
Test 6	MQH	Truss A	0.0191	50.3
Test 4	MQH	Truss B	0.0381	50.3
Test 5	MQH	Truss B	0.0381	50.3
Test 6	MQH	Truss B	0.0381	50.3

Point Source and Solid Flame Radiation Heat Flux [34]

Table A.31: Summary of validation input parameters used for WTC cases [23], radiation heat flux.

Input Parameter	Value
x (m)	0.90, 0.82, 0.71, 0.77, 1.23, 1.34, 1.23, 1.34, 1.07, 1.56, 0.57, 0.35, 0.87, 2.58
z (m)	3.3, 3.3, 3.15, 3.15, 3.46, 3.27, 0.92, 1.02, 0.13, 0.13, 3.82, 3.82, 3.82, 3.82
IOR	3, 3, -3, -3, 1, 2, 1, 2, 3, 3, -3, -3, -3, -3

Test	\dot{Q} (kW)	χ_r	A (m ²)
Test 1	2000	0.44	1.258
Test 2	2400	0.39	1.455
Test 3	2000	0.39	1.258
Test 4	3200	0.44	1.832
Test 5	3000	0.44	1.739
Test 6	3000	0.44	1.739

Ceiling Jet Temperature (Alpert) [35]

Table A.32: Summary of validation input parameters used for WTC cases, ceiling jet temperature.

Input Parameter	Value
Location Factor	1
r (m)	2, 3
H (m)	3.72

Test	\dot{Q} (kW)	T_{∞} (°C)
Test 1	2000	24
Test 2	2400	25
Test 3	2000	20
Test 4	3200	20
Test 5	3000	20
Test 6	3000	20